FABRICATION AND CHARACTERIZATION OF PIEZOELECTRIC POLYMER TRANSDUCERS

Gonzalo Aguila Flores

Supervisor : Dr. Klaus P. Kämper & Dr. Daniela Diaz Alonso

A thesis submitted for the degree of Master in Mechatronics

Thesis elaborated for CIDESI & FH Aachen

Feb 2019

Table of contents

List of Figures

List of Tables

List of Abbreviations

PVDF	Poly(Vinylidene Fluoride)
PVDF-TrFE	Poly(Vinylidene Fluoride)-Trifluoroethylene
AlN	Aluminum Nitride
PZT	Lead Zirconate Titanate
SME	Small and Medium-sized Enterprise
CAD	Computer Aided Design
TEG	Thermoelectric Generator
THF	Tetrahydrofuran
MEK	Methyl Ethyl Ketone
DMF	Dimethylformamide
NMP	N-Methyl-2-pyrrolidone
HSP	Hansen Solubility Parameters
YAG	Neodymium-doped Yttrium Aluminum garnet
SEM	Scanning Electron Microscopy
DUT	Device Under Test
JFET	Junction Field-Effect Transistor
CMOS	Complementary Metal-Oxide-Semiconductor

Declaration of Authorship

I hereby declare that I have written the present work Independently and that the sources used in this work are acknowledged as references.
The drawings or illustrations presented in this work are created by myself and if it is not the case, the images have a corresponding source proof.
This work was not previously presented to another examination board and has not been published.

Gonzalo Aguila Flores

Aachen, February 2019

Acknowledgements

First of all, I want to thank Prof. Dr. Klaus Peter Kämper for the opportunity of working with this challenging project and his support during it. Also, I would like to thank Dr. Daniela Diaz Alonso for her help and advices during the development of the project and the writing process of the thesis. Finally, thanks to the team members of the laboratory at the RTWH university in Aachen (AMO GmbH) that always helped me when I needed it.
Also, I want to express my gratitude to CIDESI and CONACYT for giving me the experience of studying and living abroad, without both institutions, this experience would never have come true.

Abstract

In this thesis work the processability of two PVDF-materials is explored and experimental routes are developed in order to build a functional sensor device. The functional prototype, based on the polymeric ferroelectric active PVDF material, is capable of sensing changes in pressure and temperature, with a strong dependency on the appropriate processing and manufacturing parameters.
After testing the influence of the fabrication methods on the ferroelectric properties, the two material variants, pure PVDF and PVDF-TrFE, are compared. Finally, the processing parameters found are implemented in the design and fabrication of a simple, yet flexible, effective force and temperature measuring device.
The experiments conducted on the fabricated device showed higher electrical responses than the majority of the devices already developed in the literature even without an amplification stage.

Chapter 1

Introduction

Marie and Pierre Curie discovered the piezoelectric effect in materials from natural origin like quartz and Rochelle salt. The discovery that a voltage can be generated over the surface of a material by applying a force or by causing a change of form in the material shape, make this property a logical choice for sensors and vice versa as actuators. Consequently, materials with this property have been implemented in different sensors as the knock sensors (vibration sensors), used for detecting the misfiring in engines, security systems, pressure gauges, microphones and many other applications. The necessity of better transducer responses has led to focusing in the search and implementation of newer piezoelectric materials as aluminum nitride (AlN) and lead zirconate titanate (PZT), which are characterized by having high voltage responses. The disadvantage of such materials is that the vast majority are ceramics and thus are brittle. This may prove to be a disadvantage for the future applications which require additional material attributes like mechanical flexibility and deposition techniques that impose less thermal stress for applications that include haptics. Here, the use of technology stimulates the senses of touch and motion in order to improve the experience of the user while handling objects; especially when it comes to virtual reality feedback. Another, on a time scale much closer applications, is the e-skin which gives a robot the ability to sense the world in a human way, transferring abilities like 'feeling' touch (pressure) and warm (temperature) objects or users in close proximity. For such applications, fortunately, a polymer PVDF has appeared which demonstrates both piezoelectric and pyroelectric properties. Such a polymer is very convenient when looking for flexible sensing materials for the upcoming applications and the relentless pursuit of smart objects. This has been pushing efforts to gain knowledge on the routes to process the polymeric materials, while at the same time improving the performance in electric signal delivery and in electromechanical transducing conversion. There are several reports in which people have tried to improve devices with the material, but most of the these only generated small output voltages of a few millivolts (usually less than 100mV). Some of the efforts to process the material note the difficulties that arise when using standard lithographic methods due to the porosity of the material and lack of adhesion.

Herein lies one focus of this work starting with research on the physical properties, methods for deposition and process integration, and analyzed by state of the art inspection methods. Two varieties of piezoelectric polymer PVDF and PVDF-TrFE will be

compared in terms of material properties, methods for producing layers, processability by standard lithography methods, and electrode metallization, followed by electrical characterization of the ferroelectric properties. In the last part, the found fabrication methods are elaborated for the generation of a functional sensor device that delivers drastically improved piezoelectric responses.

1.1. State of the art

We have had smart materials for a long time, though the term is relatively new. Some of the first smart materials were piezoelectric materials, including poly vinylidene fluoride. When a pressure is applied charges appear on the outer surfaces of the material or, in the opposite direction, they change shape (deform) when a voltage is applied over the surface of the material.
Research nowadays involves the synthesis of new smart materials, but also focuses on the application of already existing smart materials. Many applications of smart materials involve the assemblage of these material and envision new uses. Piezoelectric sensors can also be used to measure «loads» through reaction of the piezoelectric sensors to stress/strain.
Different application fields arise, since smart materials may react to different applied stimuli which could be electrical, stress/strain, pressure, thermal, light and magnetic in nature. The ability to react on stimuli is but one feature a smart material must have. The material becomes smart when it is possible to combine multiple features like the actuation and sensing properties with a device architecture. Most materials, including ceramic, alloys, and polymers, undergo volume changes as they undergo phase changes. Muscles contract and expand in response to electrical, thermal and chemical stimuli. Certain polymers, are known to change shape due to application of electric current, temperature, or changes in chemical environment. Thus, these kinds of materials open a wide horizon of possibilities to create a new smart or multifunctional sensors and actuator devices.
Most current efforts include three general types of smart materials: piezo-electric, magneto-strictive (materials that change their dimension when exposed to a magnetic field), and shape memory alloys (materials that change shape and/or volume as they undergo phase changes). Conductive polymers and liquid crystalline polymers can also be used as smart materials since many of them undergo relatively large dimensional changes when exposed to the appropriate stimulus such as an electric field.

1.2. Problem definition

There is an increasing market in flexible electronics manufactured with materials capable of multiple sensing (e.g. humidity, tactile, temperature sensing etc.). These materials are intended to fabricate electronic components integrated on flexible substrates [1][2]. Flexible sensors are expected to be thin, flexible, resistant to chemicals and durable to external forces [3]. The pursuit to meet above needs and improvements in tactile sensing capability has resulted in many kind of touch sensors, exploring numerous mods of transduction. The polymer based sensors and electronics have also been explored as they provide the mechanical flexibility and conformability, but their use is limited by the lower performance. On the contrary, transducer devices based on brittle materials like PZT, AlN, silicon as transducer report high performance but lack flexibility [4].

1.3. Justification

The increase in the necessity of reliable and high performance flexible electronics which can be used in a wide range of applications, the market share of flexible electronics is thriving high and expected to reach a billion-dollar mark by 2020 and this is one of the main reasons to develop better quality and response transducers [5]. Applications as e-Skin look for sensors capable of multiple sensing for tactile and temperature sensing. Tactile sensors based on soft piezo-polymer polyvinylidene fluoride (PVDF) and its co-polymer polyvinylidene fluoride trifluoroethylene (PVDF-TrFE) have been developed for various applications like medical sciences, robotics, space technology and more [6, 7]. The Micro and nano technology Laboratory *AMO GmbH.* located at campus Melaten in Aachen, is a non-profit SME with the mission to open way to innovations arising from convergence of technologies. The strategy to successfully pursue this mission is based on the concentration of key enabling technologies (KET) identified as the most promising source of innovations. This strategy is closely confined to innovation as intersection of discovery, invention and insight leading to economic values.
AMO is partner in the *ATLASS* European project motivated by the appealing applications scenarios. Here, considerable progress has been made in solution processing of organic materials. The integration of multilevel objects is essential if a combined sensor skin with piezo and pyroelectric properties is to be developed [8].

1.4. Objective

The objective of this work is to find process routes to integrate a specific PVDF-formula into a standard semiconductor processing environment in order to fabricate a sensor device. The ferroelectric material was to be compared to a standard PVDF material.

1.5. Specific Objectives

- Document and study the state of the art on polymeric ferro-electric materials used for piezo and pyroelectric sensing applications
- Device design: material studies and CAD design; fabrication process design and calculation of device expected values
- Build and validation of physical prototypes
- Process development for micro fabrication
- Build up appropriate analyzing procedures
- Develop circuitry needed for electrical and functional characterization
- Determine electrical properties of the material

Chapter 2

Properties of the transducer element

2.1. Ferroelectric effect

It is described as the property of some materials which are capable of sustaining a dielectric polarization under the application of an electric field. There exist a set of these material for which the crystal structure lacks a center of symmetry. This center of symmetry means that for every atom in the structure there is a point in the unit cell through which inversion will bring one to the same type of atom. A subset of the non-centrosymmetric crystals also possesses a unique axis of symmetry. These crystals are said to be polar. Polar crystals are piezoelectric (as they are acentric) and also exhibit pyroelectricity, which means that a charge separation will appear on their surfaces when their temperature is changed. Polar structures effectively have a dielectric polarization built in to the unit cell of the crystal structure. This is sometimes called «spontaneous polarization». In the figure 2.1 is found a Venn diagram summarizing the properties of the materials.

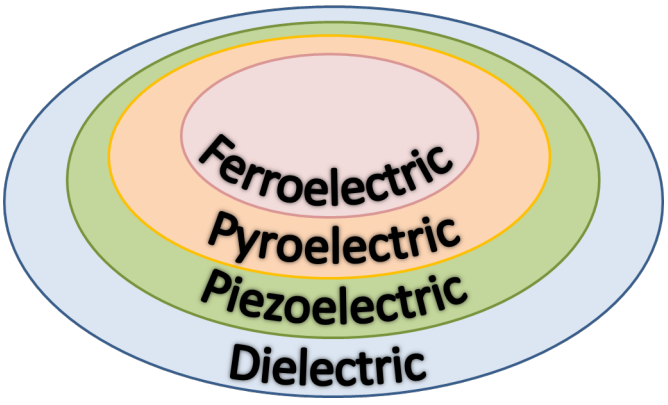

Figure 2.1: Ferroelectric materials, exhibit pyroelectricity, pyroeletric materials exhibit piezoelectricity, piezoelectric materials are always dielectrics, these relationships don't work always the other way around

A sub-set of the set of polar dielectrics exists for which the application of a field

of sufficient magnitude will cause the spontaneous polarization to switch to a different stable direction. Upon removal of the field the polarization will not spontaneously return to its original direction and magnitude. These crystals are called ferroelectric.
A reasonable working definition of ferroelectricity is «a polar dielectric in which the polarization can be switched between two or more stable states by the application of an electric field». However, as we will see in the discussion which follows, there are exceptions to this definition: some ferroelectrics are semiconducting (and thus are not dielectrics because they cannot sustain an electrical polarization); the spontaneous polarization in some ferroelectrics cannot be switched because they cannot sustain an electric field of sufficient magnitude to effect the switching, either because they reach electrical breakdown first, or because they are too conducting [9].

2.2. Pyroelectric effect

Pyroelectricity is the property of materials that have the potential to generate electrical power from thermal fluctuations and is a less well explored form of thermal energy harvesting than thermoelectric systems [10].
Energy harvesting is currently a topic of intense interest as a result of the growing energy demands of society and as a means to create autonomous and self-powered systems. For example, applications for energy harvesting devices include battery-free wireless sensor networks that do not require maintenance or replacement, with typical power requirements in the um with mW range. Methods to scavenge 'local' energy sources to generate electrical power has been considered by many researchers; examples include the use of piezoelectric materials and electromagnetic systems to convert mechanical motion into electrical energy. Other forms of ambient energy sources include light, where photovoltaics and water-splitting are being considered, wind, including the creation of micro-turbines and harvesting electromagnetic waves using antennas [10].
In the context of thermal energy harvesting, heat remains an almost ubiquitous and abundant ambient source of energy that is often wasted as low-grade waste heat. Thermoelectrics have been widely used and considered as a means to convert temperature gradients into electrical energy using the Seebeck effect. A less widely researched area is 'pyroelectric energy harvesting' In which temperature fluctuations are converted into electrical energy; although the potential to convert thermal energy to electrical energy using ferroelectric materials has been considered in the 1960's and 1970's The pyroelectric effect and potential thermal and electric field cycles for energy harvesting are explored. Materials of interest are discussed and pyroelectric architectures and systems that can be employed to improve device performance, such as frequency and power level, are described. In addition to the solid materials employed, the appropriate pyroelectric harvesting circuits to condition and store the electrical power are discussed [10].
A significant amount of waste heat is lost as a by-product of power, refrigeration, or heat pump cycles and it has been reported that in 2009 half of the energy consumed in the United States was wasted as low-grade waste heat. To harvest waste heat thermoelectric materials have attracted interests, with a number of commercial supplies of thermo-electric generators (TEG's).

Thermoelectric materials and systems generate electrical power from temperatu-

re gradients (dT/dx) while pyroelectric materials produce power from temperature fluctuations (dT/dt) and have some similarities to the way in which piezoelectric harvesters convert mechanical oscillations ($d\sigma/dt$) into electricity. Pyroelectric materials are of interest since under the correct condition they have the potential to operate with a high thermodynamic efficiency and, compared to thermoeletrics, do not require bulky heat sinks to maintain a temperature gradient. Pyroelectric harvesters tend to operate at low frequency, typically <1Hz. All pyroelectrics are polar materials and exhibit a spontaneous polarization P_s in the absence of an applied electric field. Examples of polarization include that of ionically bonded materials whereby the polarization can be a consequence of the crystal structure, while in crystalline polymers with aligned molecular chains it can be due to the alignment of polarized covalent bonds. The presence of a spontaneous polarization in the material leads to the presence of a charge on each surface of the material and free charges, such as ions or electrons, are attracted to the charged surfaces of the material. The origin of pyroelectric behavior is understood from the behavior of the surface charge as the ambient temperature is changed and assuming that the polarization level is dependent on material temperature.

If a pyroelectric is heated ($dT/dt > 0$) there is a decrease in its level of spontaneous polarization as dipoles within the material lose their orientation due to thermal vibrations. This fall in the polarization level leads to a decrease in the number of free charges bound to the material surface. If the material is under open circuit conditions the free charges remain at the electrode surface and an electric potential is generated across the material. If the material is under short circuit conditions an electric current flows between the two polar surfaces of the material. Similarly, if the pyroelectric is cooled ($dT/dt < 0$) the dipoles regain their orientation leading to an increase in the level of spontaneous polarization, thus reversing the electric current flow under short circuit conditions as free charges are attracted to the polar surfaces.

Equation 2.1 defines the relationship between pyroelectric charge (Q), generated current (i_p), rate of the temperature change (dT/dt), surface area of the material (A) and the pyroelectric coefficient (p) under short circuit conditions with electrodes that are orientated normal to the polar direction.

$$i_p = dQ/dt = p \cdot A \cdot dT/dt \tag{2.1}$$

The pyroelectric coefficient of an unclamped material, under a constant stress and electric field, is defined by the equation below 2.2.

$$P^{\sigma,E} = (\frac{dPs}{dT})_{\sigma,E} \tag{2.2}$$

where P_s is spontaneous polarization and subscripts and E correspond to conditions of constant stress and electric field respectively. While the pyroelectric coefficient is a vector quantity, the electrodes that collect the charges are often normal to the polar direction and so the measured quantity, the electrodes that collect the charges are often normal to the polar direction and so the measured quantity is often treated as a scalar. The ability of small changes in temperature to produce a pyroelectric current has been exploited for infra-red imaging and motion detection by body heat. This small electric current can also be considered for energy harvesting applications [10].

2.3. Piezoelectric effect

Since the discovery of the piezoelectric effect of crystals by Pierre and Jacques Curie in 1880, a significant progress in materials and applications in materials using the piezoelectric effect has been made. The piezoelectricity is an electromechanical phenomenon which involves the interaction between the mechanical (non-permanent deformation) and the electrical behavior of a material. A typical piezoelectric material produces an electric charge or voltage in response to a mechanical stress, also applying a voltage to the material will produce a deformation response. The former is known as the direct piezoelectric phenomenon, while the latter is known as the converse piezoelectric phenomenon. In the application, usually applying a mechanical force (stress) over the material thus generating a voltage (direct effect) is usually used in sensor technology. While applying voltages to produce deformations over the material is (converse effect) is used in actuator technology. Most of the materials and composites used as piezoelectric materials are not used raw they need some post processing in order to achieve its direct and converse properties, the most common process used is the so called poling process. Before the poling process, the piezoelectric material exhibits no piezoelectric properties, and its isotropic because of the random orientation of the dipoles, upon developing a poling voltage in the direction of the poling axis, the dipoles re-orientate to form a certain class of anisotropic structures. The piezoelectric effect is illustrated in figure 2.2, when a driving voltage with certain direction of polarity causes that the cylinder deforms being contracted. By the other way a driving voltage with an opposite polarity to the poling axis causes that the cylinder elongates.

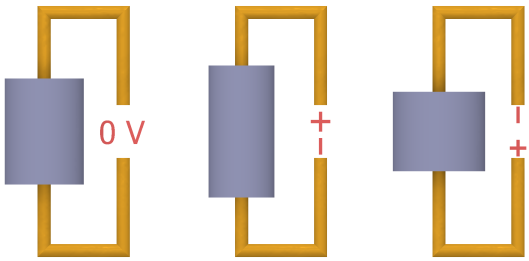

Figure 2.2: Piezoelectric Effect, the change in voltage polarization influences a shape change in the material which can be reversed by also reversing the polarity of the applied voltage

Piezoelectric materials exhibit field-strain relation. The relation is nearly linear for low electric field, which may provide many advantages when employing piezoelectric materials in system modeling and control realization. The direct and converse piezoelectric phenomena, involving and interaction between the mechanical behavior of a material, can be usefully modeled by linear constitutive equations involving two mechanical variables and two electrical variables [11]. Thus, in tensor form the equations governing the direct piezoelectric effect and the converse piezoelectric effect are written, respectively, as:

$$[D] = [e]^T\{S\} + [\alpha^S]\{E\}$$

$$[T] = [c^E]S - [e]E$$

where
$\{D\}$ is the electric displacement vector
$[e]^T$ is the transpose of the dielectric permittivity tensor
$\{S\}$ is the strain vector
$[\alpha^S]$ is the dielectric matrix at constant mechanical strain
$\{E\}$ is the electric field vector
$\{T\}$ is the stress vector
$[c^E]$ is the matrix of elastic coefficients at constant electric field strength

So far, many natural and synthetic materials exhibiting piezoelectric properties have been proposed and developed. Natural materials include quartz and Rochelle salt, while synthetic materials include lead zirconate titanate (PZT), barium titanate, lead niobate, lithium sulfate, and polyvinylidene fluoride (PVDF). Among these materials, PZT and PVDF are most popular and commercially available [11].
Both classes of materials are available in a broad range of properties to suit diverse applications. PZT is normally used as actuators, while PVDF as sensors. One of the salient properties of PZT or PVDF is that it has very fast response characteristic to the voltage, and hence wide control bandwidth. In addition, we can fabricate simple, compact, low power-consuming devices ($<$10W) featuring a set of piezoelectric actuators and/or sensors.

2.4. Dielectrics

Dielectrics are insulating materials or very poor conductors of electrical current. When dielectrics are placed in an electric field, practically no current flows in them because, unlike metals, they have no loosely bound, or free, electrons that may drift through the material. Instead, electrical polarization occurs. The positive charges are displaced minutely in the direction of the electric field, and the negative charges are displaced minutely in the direction opposite to the electric field. This slight separation of charge or polarization, reduces the electric field within the dielectric [12].

Chapter 3

Materials

3.1. PVDF

The first polymeric ferroelectric to be discovered was polyvinylidene fluoride (PVDF). The monomer for this possesses the formula CH_2CF_2. It was first shown to be piezoelectric by Kawai [13] and later Bergman et al. [14] speculated about the possibility of it being ferroelectric, although no Curie temperature could be shown to exist, as the polymer melts first. The structure of the polymer is complex, as the polymer backbone can adopt a number of configurations depending upon whether the neighboring carbon-carbon linkages adopt trans or gauche configurations. In a trans (T) configuration, the groups bonded to the carbon atoms sit on the opposite sides of the carbon-carbon bond. In a gauche (G) configuration, they sit on the same side. In an all-trans configuration, the carbon backbone of the polymer forms a simple zigzag. In the case of PVDF, there are four different phases with different T and G sequences, and with different ways the polymers stack together in crystal structures. The polymer crystallizes from the melt into form II, also called α-phase, in which the bonds arrange themselves into the sequence $TGTG$. The fluorine atoms are strongly electronegative which makes the $C-F$ bond polar so that the molecule has a net dipole moment perpendicular to its length. However, the molecules of polymer arrange themselves in the unit cell so that the dipoles cancel each other out. Form II is neither ferroelectric nor piezoelectric, but application of an electric field will convert it into form II_p, also called the delta-phase, in which the polymer molecules are arranged so that the unit cell has a dipole moment. High-temperature annealing of either of these forms will produce form III the (γ-phase), which has a new $TGTTTGTT$ configuration which also has a net dipole moment perpendicular to the long axis of the molecule and these arrange in a crystal structure which is also polar. Subjecting forms II or III to stretching or drawing will produce form I (the β-phase), which is an all-trans configuration. It can be seen from the figure below that of the three molecular configurations, the polar bonds all point most-nearly in the same direction and this is retained in the unit cell. Electrical poling makes this the most strongly piezoelectric phase of PVDF [9]. All the possible phases of PVDF are illustrated in 3.1.

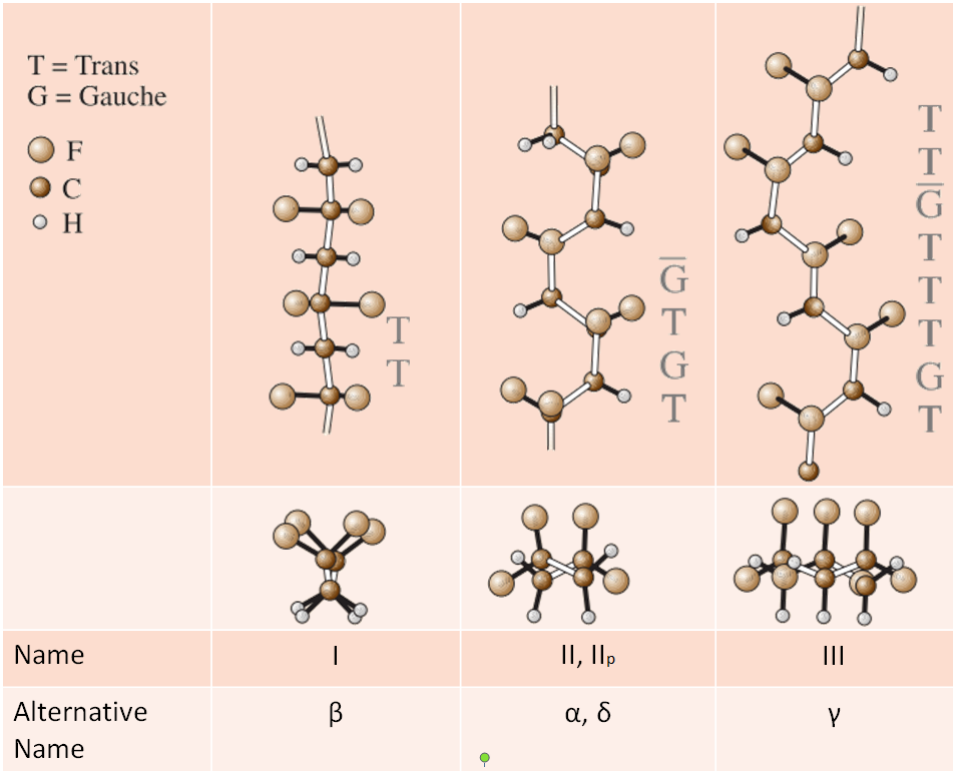

Figure 3.1: Existing phases of PVDF [9]

3.2. PVDF-TrFE

Depending on the sample preparation conditions, PVDF exhibits at least four different crystalline forms at ambient temperature. PVDF-TrFE copolymer has a definite T_c and exhibit a single ferroelectric β-crystalline structure at ambient temperature far below its T_c. Spinning processes assists in preferentially orienting the $C-F$ dipoles in PVDF. It is well known that heating the poled copolymer sample above its T_c results in the depolarization of its dipoles, and hence the electrospun nanofiber is thermally treated to $130°C$, which is well below its melting temperature ($T_m \approx 147°C$) but above its T_c ($\approx 115°C$)

In some studies over FTIR spectra of PVDF-TrFE samples, solid films of the copolymer showed absence of peaks in the alpha-phase (α) but presence of peaks in the beta phase, which is an evidence that the PVDF-TrFE sample can directly crystallize into the ferroelectric beta-phase (β) from its melt [15].

Homopolymer PVDF has a lower crystallinity than PVDF copolymers have [16], this is one of the reasons why this copolymer is being used to produce piezoelectric films. (PVDF-TrFE always produces β-phase, in certain quantities, but additional poling process is required in order to produce big quantities of the required phase)

3.2.1. Poling

The piezoelectric effect originates from induced polarization. To induce polarization, the dipoles in a semi-crystalline polymer such as PVDF must be reoriented through

the application of a strong electric field at elevated temperature. The temperature is then lowered in the presence of the electric field so that the domains are locked in the polarized state. The material's piezoelectric effect is directly related to the degree of polarization achieved. The two most common techniques to induce polarization in piezoelectric polymers are electrode and corona poling.

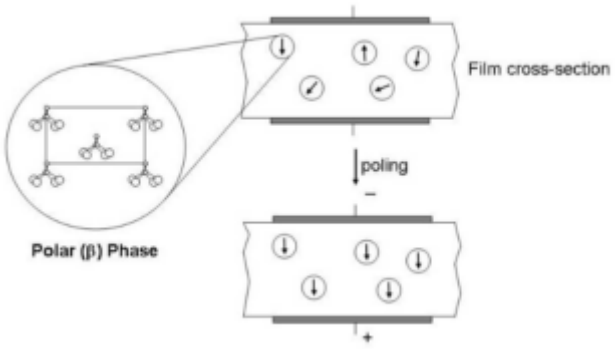

Figure 3.2: Reorientation of the β-phase dipoles in PVDF via poling

A schematic diagram of the electrode poling method is presented in the figure below. The conducting electrodes, which are either evaporated, sputtered, painted or pressed on the polymer surfaces, are necessary for poling. For poling of PVDF films, a 600 Å layer of evaporated aluminum on each side has been found to work satisfactorily. The voltage potential applied to the electrodes produces an electric field across the sample. To prevent arcing that will permanently damage the material, the sample may be placed in a vacuum or submerged in an insulating fluid such as Fluorinert, or alternatively if the electrodes do not reach the edge of the film the poling can be done in air without arcing. Permanent electrodes which could be evaporated, sputtered or painted are preferred over the pressed-on electrodes because of the superior contact between the electrodes and the sample. The poor contact in the case of pressed electrodes may lead to local discharges, dielectric breakdown or inhomogeneities in the poling field. The sample should be monitored for contaminants as the charges may get injected into the material at high electric and thermal fields.

Both constant and varying electric fields can be applied to the sample during electrode poling. A constant electric field is held on the sample from 10-30 minutes up to 2 hours. Application of high voltages for a prolonged period of time may increase the probability of dielectric breakdown thus making a variable field procedure a more attractive alternative. The process when the material is poled through the application of a variable electric field is called «hysteretic poling». The varying electric field is usually applied at low frequency (mHz) and either sinusoidal or triangular waveforms may be used. Bauer [17] proposed the application of an alternating electric field E, with a frequency which could range from 0.001 to 1 Hz, and which is made to increase gradually and in a cyclic way between $\pm 0 E_N$, where E_N should be slightly in excess of the coercive force E_c for the used material.

The schematic diagram for corona poling is presented below. A surface is placed on a heating plate with the bottom surface connected to the ground. A corona tip (a needle or a sharp blade) is suspended above the sample and is subjected to high (8-10 kV) voltages. The dry air at the tip gets ionized with the tip's polarity. When the

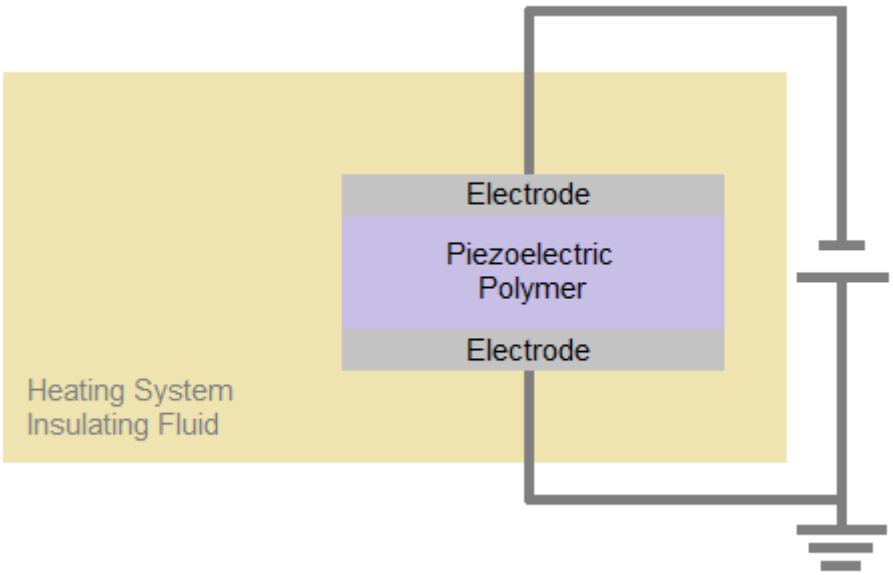

Figure 3.3: Schematic of the electrode poling system

corona discharge occurs, the ionized particles are accelerated towards the ground and are deposited on the sample´s top surface. The charges remain on the surface generating a poling electric field between the top surface and the ground. The magnitude of the electric field depends on the amount of charges deposited that can be controlled with a metallic grid placed between the corona source and the polymer. The grid is usually placed at the distance of 3-4 mm from the sample. The voltage on the grid may vary from 0.2 to 3 kV. The advantages of the corona poling are that it is more amenable to film imperfections, electrodes are not required, and large area samples may be poled. The disadvantage is that it is considerably more difficult to setup and optimize than the direct electrode method.

The magnitude of the electric field and sample temperature are important parameters in the poling process. The usual rule of thumb is the higher the applied electric field, the higher the induced polarization provided the poling field is larger than the coercive field of the material being poled. The coercive field for PVDF and its copolymers is typically between 50 and 120 MV/m (120 V/μm). Although the poling may be done at room temperature, an elevated temperature improves dipole mobility and consequently increases the material polarizability. Another issue to consider is warping of the films during the poling process due to the change in volume during orientation of the dipoles. Poling at elevated temperatures can help minimize warping due to relaxation of the polymer film and help it conform the «new» poled volume, especially at the boundary between the poled and non-poled areas. Unlike the poling field for which larger values will produce larger polarization, there is an optimum poling temperature that results in maximum polarization and piezoelectric properties. Typical optimum poling temperatures are in the range 85°C to 130°C [18]. Means for polarizing ferroelectric materials up to a predetermined polarization level include the application of an electric field E to these materials.

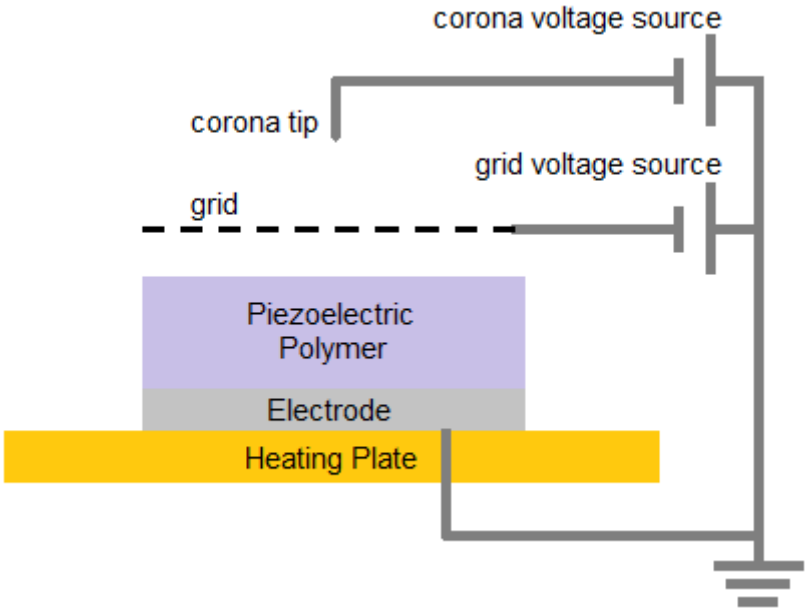

Figure 3.4: Schematic of the corona poling system

3.3. Solvents

A solvent is a liquid that dissolves a solute. The solvent is the component of a solution that is present in greater amount. Perhaps the most common solvent in everyday life is water. Many other solvents are organic compounds, such as benzene, tetrachloroethylene, or turpentine.

At the molecular level, solubility is controlled by the energy balance of intermolecular forces between solute-solute, solvent-solvent and solute-solvent molecules. Recall from general chemistry that intermolecular forces come in different strengths ranging from very weak induced dipole - induced dipole interactions to much stronger dipole-dipole forces (including the important special case, hydrogen bonding). However, there is a simple, very useful and practical empirical rule that is quite reliable. That simple rule is «like dissolves like» and it is based on the polarity of the systems i.e. polar molecules dissolve in polar solvents (e. g. water, alcohols) and non-polar molecules in non-polar solvents (e.g. the hydrocarbon hexane). This is why ionic compounds like table salt (sodium chloride) or compounds like sugar, dissolve in water but do not dissolve to any great extent in most organic solvents. It also applies to the separation of oil and water (e.g. in salad dressings). The polarity of organic molecules is determined by the presence of polar bonds due to electronegative atoms (e.g. N, O) in polar functional groups such as amines ($-NH_2$) and alcohols ($-OH$) [19]. It has been reported that solvents produce effects on the properties of PVDF films. Polar solvents are typically used for PVDF solutions such as tetrahydrofuran (THF), acetone, MEK, dimethylformamide (DMF), and NMP, which are divisible into two categories: highly polar (DMF and NMP) and lowly polar (THF, acetone and MEK). In Zhu's report is told that highly polar solvents as NMP with polarity index (PI) of 6.7 are good solvents of PVDF, for reference the polarity index of water is 10.2. MEK with a PI of 4.7 has a lower polarity index and is a good swelling agent of PVDF at room temperature [16]. In literature Sencadas attributed the slower evaporation rate of the DMF solvent (153°C)

to the presence of high bead formation in PVDF and its related polymers. DMF:MEK solvent mixture is mostly preferred to dissolve PVDF-TrFE due to their thermal and electrical characteristics: DMF shows a high dielectric constant (38.2), whereas MEK has a lower boiling point (80°C), which allows faster polymer crystallization. The most popular solvent in the literature is DMF, because the high solubility of PVDF in this material, despite such properties, DMF is a dangerous material and with possibly carcinogenic risk for humans. As discussed before similar polarities tend to be suitable solutes and solutions. In tables it is demonstrated that N, N Dimethylformamide has a polarity index (P') of 6.4 and in most literature it results to be the most suitable and widely used solvent, but also due to their polarity index Dimethylacetamide ($P' = 6{,}5$) and N-Methylpyrrolidone ($P' = 6{,}7$) and any other available solvent near that polarity index could be able to dissolve PVDF. For PVDF-TrFE the favorite solvent is MEK with a polarity index of 4.7, it could be expected that the following solvents could work, Methyl Isobutyl Ketone ($P' = 4{,}2$), Ethyl Acetate ($P' = 4{,}4$) [20].

3.3.1. Hansen Solubility Parameters (HSP)

Hansen Solubility Parameters (HSP) are a simple, numerical way to describe solubility and compatibility with polymers, solvents, particles etc. HSP does this with three intuitive numbers, δ_D for Dispersion, δ_P for Polar and δ_H for Hydrogen bonding. These three numbers are capable of explain why a solvent can dissolve certain solutes. The three HSP numbers determine if a determined solute is soluble into a determined solvent, the closer the HSP values of the solvent to the HSP values of the solute, the better solvent it is [21].

3.3.2. Solvent Blends

A blend of two solvents can often have better solubility properties (lower HSP Distance) than either of the individual solvents which might even be non-solvents for the target materials.
One man can choose a target polymer, then various pairs of solvents and vary their ratio till you get the best match (lowest HSP Distance or R_a).
When Charles M. Hansen first came up with his HSP scheme he saw that it made a surprising prediction. That two bad solvents represented as the blue dots in the image below 3.5, on the opposite sides of the HSP Sphere should produce an excellent solvent (green dot in the middle) when mixed 50:50. If his HSP ideas were wrong then mixing two bad solvents would create another bad solvent. When he did the test his ideas were confirmed. It is possible to elaborate a good solvent from a mixture of bad ones.

It is one of the most useful ideas behind the Hansen Solubility Parameters (HSP). It allows formulators amazing freedom to combine solvents that are attractive in terms of cost, safety, odor, volatility, etc. but which are poor solvents for the specific system and create an excellent solvent blend. By being smart with the relative volatilities of the solvents it is possible to make mixes that deliberately crash out the solutes when evaporation starts (the best solvent is more volatile) or, alternatively to make a super-smooth coating by ensuring that the best solvent for the critical component is the least volatile so keeps it in solution up to the last moment.
In most literature PVDF is dissolved in DMF, the problem related to DMF and some

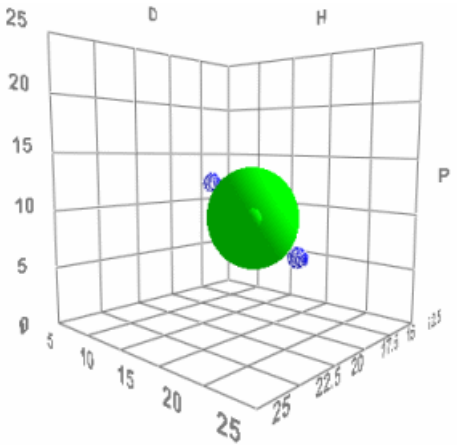

Figure 3.5: Spatial representation of solubility parameters δ_D, δ_P and δ_H

other materials is that they are dangerous for human handling and they imply poisonous and mutagenic risks, so for that reason it couldn´t be considered as an available solvent, instead from HSP parameters of various materials in the laboratory, it was determined that mixing 50/50 of Dimethyl Sulfoxide (DMSO) with Acetone would create a solvent with similar characteristics to DMF. DMSO is a solvent used in pharmaceutical industry and declared harmless for humans, acetone as well is harmless with the proper handling.

Chapter 4

Fabrication Methods

4.1. Procedurals to film and sheet fabrication

There are three possible techniques to fabricate polymer films, by solution casting or by melt, or sinter fabrications.

4.1.1. Solution casting

The basic idea in solution casting is to dissolve the polymer in a suitable solvent to make a viscous solution. The solution is then poured onto a flat, non-adhesive surface, and the solvent is allowed to evaporate. The dry film can then be peeled («stripped») from the flat surface.
One of the principal differences between high polymers and low molecular weight compounds is that polymers will form films, whereas small molecules are deposited as crystals or weak conglomerates. Thus, it is sometimes possible to confirm the formation of a high polymer by the fabrication of a strong, cohesive film. On a laboratory scale, the solution casting of films is quite easy. Usually, the first problem is to find a suitable solvent for the polymer. A preferred solvent is one which is sufficiently volatile that it will evaporate at a reasonable rate at room temperature or slightly above, but not so volatile that it evaporates rapidly and forms bubbles or semi-crystalline precipitates. Rapid volatilization also causes cooling of the film, which could cause crazing or condensation of water from the atmosphere. A solvent that has a boiling point between about 60 and 100°C will usually give good films. If the casting procedure is to be carried out on an open laboratory bench, some consideration should be given to the potential toxicity or flammability of the solvent. On an industrial scale, the polymer solution is fed continuously through a slit die onto a large rotating drum, or onto a moving metal belt a hood assembly may be used to remove organic solvents from the work area. Films of poly(vinyl alcohol), poly(vinyl chloride), or vinyl chloride copolymers are often manufactured by the use of these techniques [22].

4.1.2. Melt Pressing of film

Polymers that are thermally stable above their melting or softening temperatures can be fabricated into films by a combination of heat and pressure. The melt pressing technique is more often used in the laboratory than in the manufacturing plant because large films are difficult to prepare by this method, and the process is discontinuous rather than continuous. The apparatus employed consists of two electrically heated platens. One platen can be forced against the other by means of a hydraulic unit (usually hand-pumped). The powdered or subdivided polymer is placed between two sheets of aluminum or copper foil, and this sandwich is placed between the two heated platens. Pressure is then applied, whereupon the sandwich is removed and cooled, and the film is separated from the foil. In practice, the temperature is too high, the polymer will simply flow out of the sandwich. If the temperature is too low, the film may be opaque or weak because of inadequate fusion. Metal shims or gaskets can be used in the sandwich to define the thickness of the film.

4.1.3. Sinter fabrication of film

Some polymers, such as poly(tetrafluoroethylene) (Teflon), have melting points that are so high that melt fabrication techniques at high pressures are not feasible. However, powders of such polymers can be «preformed» into weak films at high pressures. Subsequent heating above the melting point completes the sintering process.

4.1.4. Melt extrusion of film

Preferred manufacturing processes are those which are continuous. Melt extrusion processes have this advantage. The overall sequence of operations is as follows. Polymer pellets or powder are fed into a screw extruder. This is a device that heats the polymer and, by means of a rotating screw spindle, forces it under pressure into the die. The molten polymer is then extruded through the die slit. The flat sheet of molten polymer is then extruded through the die slit. The flat sheet of molten polymer is collected by a rotating drum, which cools the film to below the softening temperature. Subsequent rollers complete the cooling and orientation processes.

4.1.5. Bubble blown films

An alternative method for the melt extrusion of films involves the extrusion of a tube of polymer, which is then expanded by compressed gas to form a tube of thin film. Molten polymer from a screw extruder is forced through an annular die. Gas pressure inside the extruded tube blows the tube into a cylindrical bubble. The bubble is flattened by rollers, slit lengthways to form a continuous film, and then wound into a roll. Film made in this way has a high degree of biaxial orientation. Copolymers of vinyl chloride and vinylidene chloride can be fabricated into films by this technique.

4.1.6. Films by calendaring

The process of calendaring consists of squeezing molten polymer into a thin sheet between heated rollers. This method normally used for the manufacture of thick films (0.05-0.25 mm). It is a process much used for poly (vinyl chloride) and related copolymers.

4.1.7. Films by spin-coating

With high resemblance to solution casting films, except the films are produced by pouring the viscous solution onto a flat rotating surface, the surface can be static or in movement at the moment of pouring the solution. The thickness of the films is controlled by the spin-speed and the concentration of the solution. Films presented in this work will be fabricated under this method.

Chapter 5

Experimental characterization

5.1. Profilometry

With the profile method, a surface is sampled with a fine diamond tip along a line, recording a height profile. Numerous surface morphology parameters can be determined from the height profile, such as roughness, waviness, the height histogram, skewness and slope of the height distribution, mean local surface pitch, contact ratios and so on [23]. Film thicknesses can be determined very quickly, easily and precisely through the preparation of a step and the application of the profiler.

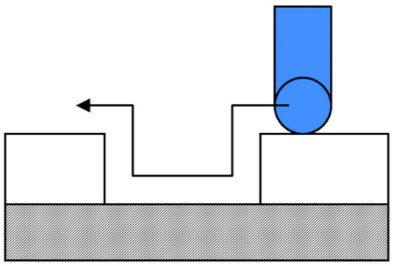

Figure 5.1: Representation of the execution of the profilometry scan [23]

Profilometers consist of at least two parts a detector and a sample stage. The detector is what determines where the points on the sample are and the sample stage is what holds the sample. In some systems, the sample stage moves to allow for measurement, in others the detector moves in some both move [24].

There are two main types of profilometers: contact (stylus) and optical. Stylus profilometers use a probe to detect, or physically 'feel' the surface. Physically moving a probe along the surface in conjunction with a feedback loop to maintain a constant force which allows for the acquisition of surface height and roughness information along the scan line [24].

Optical profilometry uses light instead of a physical probe, the key component to this technique is directing the light in a way that it can detect the surface in 3D,

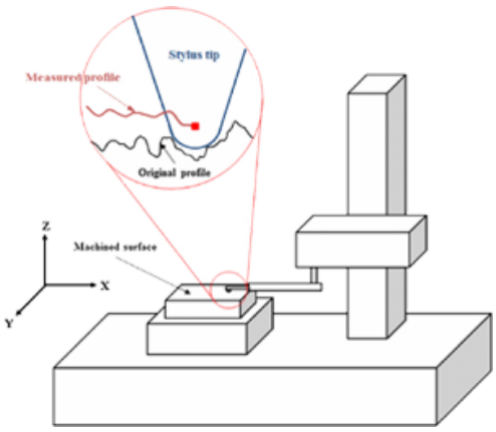

Figure 5.2: Stylus profilometer set-up

this can be done by different methods. Examples of optical profilometry include white light interferometry, scanning confocal microscopy, and grid confocal. Since optical profilometers use a photo-diode array as the detector they are able obtain data over a 2D area. Stylus profilometers use a probe as the detector so they obtain data along the length of a 1D line. Since optical profilometers can obtain height (z) information over an area, this means that optical profilometers are 3D techniques while stylus profilometry is a 2D technique. [24]

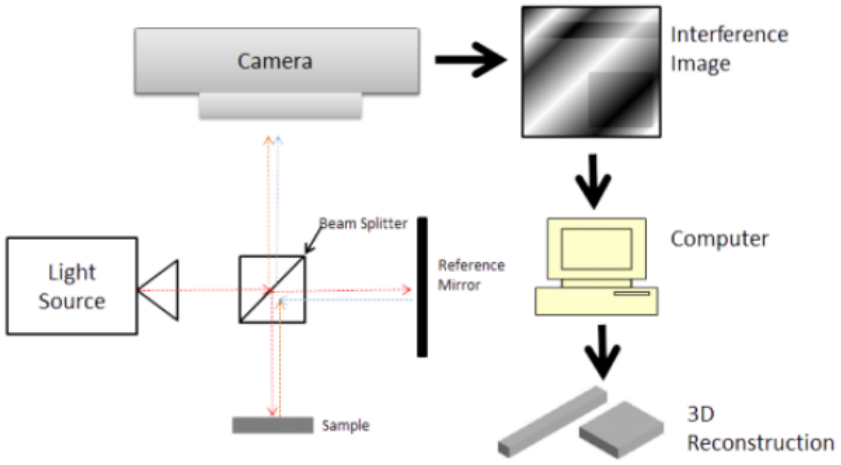

Figure 5.3: Schematic of interferometric profilometer [24]

5.1.1. Description of the instruments available

Inside the institution it is found a DekTak3ST system which takes measurements electromechanically by moving a diamond tipped stylus over the sample surface according to a user-programmed scan length, speed, and stylus force. The stylus is linked to a Linear Variable Differential Transformer (LVDT), which produces and processes

electrical signals that correspond to surface variations of the sample. After being converted to a digital format, these surface variations are stored for display and analysis [25].

5.1.2. Limitations of the stylus

The stylus shape may have an impact on the measurement data as it is the component that makes direct contact with the sample's surface. When measuring samples with narrow trenches, the stylus is unable to correctly verify the widths or reach the bottom of the trench. This is because the width of the stylus is caught at the opening. To ensure an accurate measurement of the thickness of the films it is always required to have big enough trenches to compare the heights between surface and the trenches [25].

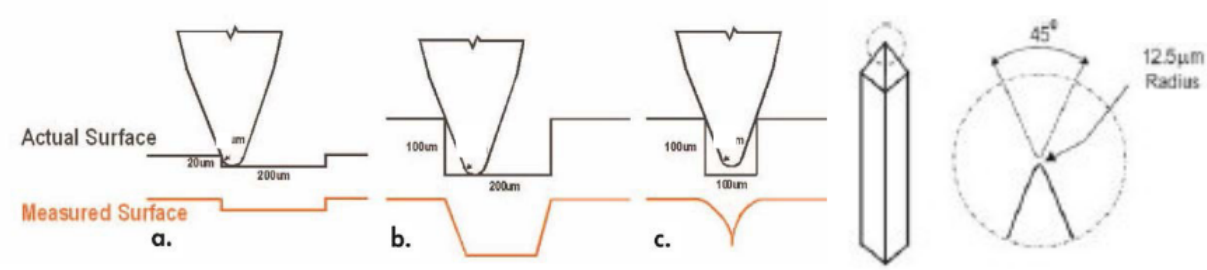

Figure 5.4: Geometry of stylus and its influence over height measuring

5.2. Ellipsometry

Film thickness can be measured by breaking the samples through a cross section and perform scanning electron microscopy (SEM) to measure the thickness of the layers. However, this method is destructive and time consuming, and it is difficult to prepare the sample. After the deposition of nanometer-thick fluorocarbon films, it is important to measure the polymer film thickness. Without knowing the deposited thickness, it is hard to develop and qualify the anti stiction film nanoimprinting.
Spectroscopic ellipsometry is a nondestructive and very sensitive measurement technique that uses polarized light to characterize thin films surfaces, and material microstructure. Its operation principle consists in the determination of the relative phase change in a beam of reflected polarized light. The figure 5.5 illustrates the basic principle behind ellipsometry. First, the polarization state of incoming light is known. This incident light interacts with the sample and reflects from the surface. The interaction of the light with the sample causes a polarization change in the light from linear to elliptical polarization. The polarization change, or a change in the shape of the polarization, is then measured by analyzing the light reflected from the sample.
Ellipsometry measures two values, psi(Ψ) and delta (Δ), that describe this polarization change. These values are related to the ratio of Fresnel reflection coefficients, R_p and R_s for $p-$ and $s-$polarized light, respectively, as shown in the equation 5.1:

$$\rho = \tan(\psi)e^{i\Delta} = \frac{R_p}{R_s} \tag{5.1}$$

Because ellipsometry measures the ratio of two values, its is highly accurate and very reproducible. The ratio is a complex number, this it contains «phase» information, delta, which makes the measurement very sensitive.

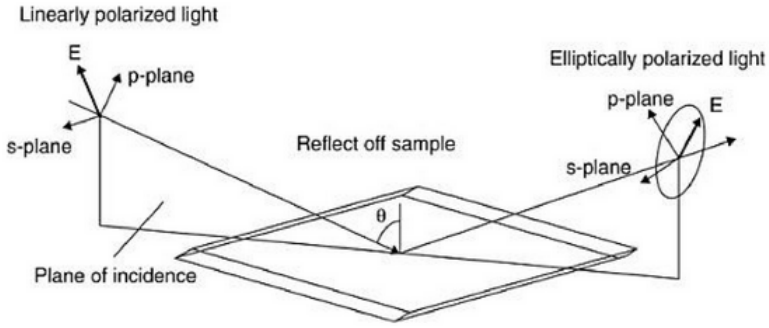

Figure 5.5: Basic principle of ellipsometry

Ellipsometry does not directly measure optical constants or film thickness but psi and delta are functions of these characteristics. These two values by themselves are not very useful in characterizing a film. What we really want to know are properties such as film thickness, optical constants, refractive index, and other useful data. These characteristics are found in the well known Fresnel equations and algorithms to produce a model that describes the interaction of light with the sample. These optical parameters are then matched to computer models to determine the structure and composition of the sample [26].

5.3. Raman spectroscopy

«Vibrational spectroscopy includes several different techniques, the most important of which are mid infrared (IR), near-IR, and Raman spectroscopy. Both mid-IR and Raman spectroscopy provide characteristic fundamental vibrations that are employed for the elucidation of molecular structure» [27].

One of the ways to compare the properties of the elaborated film is through Raman Spectroscopy, which is an appropriate method to find vibrational spectra capable of describe the constitution of the material (e.g. chemical composition and phase of the material). The Raman vibrational bands are characterized by their frequency (energy), intensity (polar character or polarizability), and band shape (environment of bonds). Since the vibrational energy levels are unique to each molecule, the IR and Raman spectrum provide a «fingerprint» of a particular molecule. The frequencies of these molecular vibrations depend on the masses of the atoms, their geometric arrangement and the strength of their chemical bonds [27], especially in materials as polymers and ceramics. Thus, this would be helpful to find the constitutions of alpha and beta phase in the spin-spin coated films.

5.3.1. Instrumentation of a Raman Spectrometer

Raman instrumentation must be capable of eliminating the overwhelmingly strong Rayleigh scattered radiation while analyzing the weak Raman-scattered radiation. A Raman instrument typically consists of a laser excitation source (UV, visible, or near-IR), collection optics, a spectral analyzer (monochromator or interferometer), and a detector. The choice of the optics material and the detector type will depend on the laser excitation wavelength employed [28]. The figure below 5.6 represents the technical diagram of a Raman spectrometer.

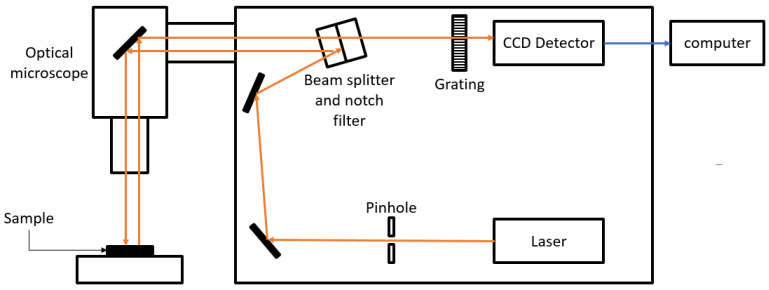

Figure 5.6: Technical diagram of a Raman spectrometer

5.3.2. Sources

The sources used in modern Raman spectroscopy are nearly always lasers because their high intensity is necessary to produce Raman scattering of sufficient intensity to be measured with a reasonable signal to-noise ratio. Five of the most common lasers along with their wavelength used for Raman spectroscopy are; Argon ion (488 or 514.5 nm), Krypton ion (530.9 or 647.1 nm), Helium/Neon (632.8 nm), Diode laser (782 or 830 nm) and Nd; YAG (1064 nm). Because the intensity of Raman scattering varies as the fourth power of the frequency, argon and Krypton ion sources that emit in the blue and green region of the spectrum have an advantage over the other sources.
Diode and Nd:YAG laser which emit near-infrared radiation are used as powerful excitation sources. Near-infrared sources have two major advantages over shorter wavelength lasers. The first is that they can be operated at much higher power (up to 50W) without causing photodecomposition of the sample. The second is that they are not energetic enough to populate a significant number of fluorescence producing excited electronic energy states in most molecules. Consequently, fluorescence is generally much less intense or nonexistent with these lasers. The Nd/YAG line at 1064 nm is particularly effective in eliminating fluorescence. The two lines of the diode array laser at 782 and 830 nm also markedly reduce fluorescence in most cases [28].

The laser radiation is directed to the sample by means of a lens and a parabolic mirror and the scattered light from the sample is collected and passed to a beam splitter and to the moving mirrors. It is then passed through a series of dielectric filters and focused onto a liquid nitrogen cooled detector [28].

5.3.3. Filters

Liquid filters are placed between the source and the samples tube. Different filters are used for different excitation radiation. Filters made of quartz glass or nickel oxide glass is used for getting monochromatic radiations. The functions of filters are to isolate a single exciting line, to remove high energy radiation that might cause photodecomposition or fluorescence and to remove the continuous spectrum in the region occupied by the Raman lines.

5.3.4. Monochromators

In the monochromator, both lenses and mirrors have been used. Most Raman spectrometers use a diffraction grating as the dispersing element. A grating instrument has a wide aperture and a medium dispersion. A double monochromator is used to avoid stray light problem from scattering by dust particles in the sample [28].

5.3.5. Detectors

Raman spectrum can be photographed with an ordinary spectrograph. Basically there are two different ways to detect and record Raman lines. The easiest way is to gather the scattered light emerging through a glass window at the end of the Raman sample tube. It is passed through a prism or grating and then focused on a photographic plate. The plate is then developed and both the line frequencies and intensities can be measured using external equipment. Modern spectrometers which have photomultiplier tubes are direct measurements and facilitate automatic scanning of a spectrum. The spectrum produced by the monochromator is passed through a slit which allow a narrow wavelength region to pass through which is focused on to a photomultiplier type detector. This detector employs an amplifier and a recorder. It directly provides the Raman spectrum [28].

5.3.6. Sample handling

Sample handling techniques for Raman spectroscopic measurements is simpler than for infrared spectroscopy because glass can be used for windows, lenses and other optical components instead of the more fragile and atmospherically less stable crystalline halides. In addition, the laser source is easily focused on a small sample area and the emitted radiation efficiently focused on slit. Consequently, very small samples can be investigated. In fact, a common sample holder for non-absorbing liquid sample is a glass melting-point capillary [28].
For the samples that could be prepared in the studies in this text we consider to handle liquid samples for the solutions and solid samples for the already casted films. Raman spectroscopy for liquids can be recorded as neat or in solution. Commonly small quantities of liquid about 0.3 ml of a liquid may be required, the sample can be taken in glass or silica containers or capillaries. The spectra can be measured directly from the reaction vessel. Water is a good solvent for recording the Raman spectra. Water absorbs strongly in the infrared but it gives a poor Raman scattering. Thus Raman spectroscopy is a valuable tool for studying water soluble biological material.

For solids Raman spectra can be recorded for polycrystalline materials or monocrystalline materials. No medium is required such as null, KBr or solvent is needed. A few milligrams of the solid samples are required. Solid can be packed into a capillary tube as a powder. The crystal can be mounted in a goniometer on a glass or silica fiber. The spectra can be measured for different orientation of the crystal. For a single crystal, the Raman spectrum varies depending on the direction of the crystal axis, when is polarized light is used as incident radiation. Raman spectra of adsorbed species can be recorded at different temperatures and pressures [28].

5.3.7. Interpretation of spectra

The assignments of fundamental modes of vibrations and interpretations of the spectra have been carried out by following empirical correlation of group frequencies, infrared and Raman selection rules, the magnitude and relative intensities of the spectra. In the case of polyatomic molecules, the interpretation of spectra is highly complex due to the appearance of combination and overtone bands this could be also shown in [29] [28].

5.3.8. Raman Analysis of PVDF

PVDF may exhibit four crystalline phases, named alpha, beta, gamma and delta phases, among which the polar beta phase is of special interest due to its large pyro- and piezoelectric activity. The non-polar alpha-phase is the most common one, since it can be obtained directly from the melt [30].
Depending on the preparation conditions of PVDF there are usually three main crystalline forms which have distinct molecular conformations. The unit cell of form I (β-phase) contains polymer chains with an all trans structure while that of form II (α-phase) presents Trans-Gauche sequences. An intermediate conformation, consisting in sequences of three Trans-bonds separated by a Gauche bond, is found in the case of form III (γ-phase) [31].
The crystallization of PVDF in the beta phase directly from the melt is not straightforward, and the most common method to achieve the conformation of PVDF into beta phase are the mechanical deformation (stretching) of PVDF films in the alpha phase. Other less frequent methods are poling which consists in the application of very intense electric fields to a PVDF film, annealing at temperatures above the glass transition temperature or casting PVDF solutions into a solid substrate at controlled temperatures [30].
Raman spectra is as discussed in Larkin's book, capable to find the specific vibrational bands of the materials, which are characterized by their frequencies, intensity and band shape, since the vibrational energy levels are unique to each molecule, the Raman spectrum provides a fingerprint of a particular molecule.
The interpretation of the vibrational spectra is performed through two possible approaches, the first one is based on the use of the group theory with mathematical calculations of the forms and frequencies of the molecular vibrations. The second one performs the use of empirical characteristic frequencies for chemical functional groups. Many empirical group frequencies have been explained and refined using mathematical theoretical approach. In general, many identification problems are solved using the

empirical approach. Certain functional groups show characteristic vibrations in which only the atoms in that particular group are displaces.
The PVDF exhibits the following expected features: vibrational modes at 480 cm^{-1} and 611 cm^{-1}, these modes are mainly due to CF_2, only the CH_2 exhibits a bending mode at about 1430 cm^{-1}, this band is present in all crystalline forms, only form II (α) present a significantly large number of characteristic bands, from which the one at 795 cm^{-1} is particularly intense and well defined. For the case of forms, I (β) and III (γ) present a smaller number of bands that are generally very weak and fairly similar [31]. Two characteristic and well defined band appear at the region around 800 cm^{-1} , the first one at 839 cm^{-1} which has been frequently discussed in previous experimental analyses [30]-[32], this band is common to beta and gamma phases but is very strong only in the first case, while the 811 cm^{-1} band is only characteristic of form III (γ) but its intrinsically weak.

5.4. Electrical characterization

Due to the non-linear behavior of ferro-electric materials like PVDF, standard electrical measurements are not achieved with consistent repeatability, making it necessary to perform different kinds of measurements. The most common way to perform such analysis with ferroelectric materials is with a Sawyer-Tower circuit or with specialized tools dedicated to measure ferroelectric and piezoelectric properties of the materials. The most extended measurement devices are provided by *Radiant Technologies inc.* Radiant Technologies offers a wide range of Precision Non-Linear Test Systems which can be used to measure different properties of piezoelectric materials.

The basic Sawyer-Tower circuit consists of an excitation source with either sinusoidal or triangular waveform and a testing capacitor C_0 to collect the current of the ferroelectric device C_x. The voltage of the device is introduced in an oscilloscope as the X axis and the integrated current of the device is introduced as an expression of the charge of C_x in the Y axis.

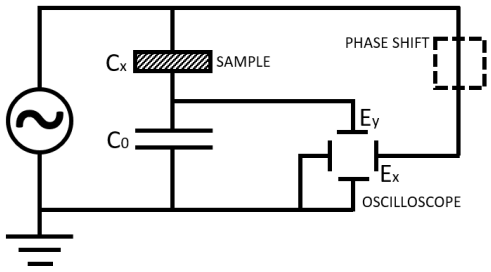

Figure 5.7: Sawyer-Tower circuit basic diagram

Chapter 6

Processing

6.1. Spin-coated films

All the films presented in this work were fabricated by spin-coating of PVDF solutions. Spin-coating is the primary coating method used in semiconductor production. The solutions applied were PVDF-TrFE from PIEZOTECH and pure PVDF from Sigma-Aldrich, two very different materials that are compared during the following chapters. The PVDF-TrFE can be dissolved in MEK, but standard PVDF (Sigma Aldrich) can only be dissolved in DMF. Due to the toxicity of DMF it was not possible to use such material in the laboratory. Tests performed using different solvents in the laboratory to dissolve the Sigma-Aldrich PVDF pellets included acetone, DMSO, acetone combined with MIBK, ended in inappropriate results. Using the before mentioned Hansen-Solubility parameters it was possible to find an optimal combination that could be used to dissolve the standard PVDF. This mixture was composed of 50 % acetone and 50 % DMSO. To prepare the solutions for the PVDF-TrFE (powder) and of the standard PVDF (pellets) the materials were tared and placed inside of flasks, adding the corresponding quantity of relevant solvent to achieve solutions of 10 % in weight (wt). The mixtures were magnetically stirred on a hotplate at a temperature of 50°C to ease the dissolution of the material. The mixtures were stirred for 1 hour to achieve complete dissolution, to ensure homogeneity the solution was sonicated for 10 minutes. To spin-coat the films it was necessary to perform cleaning processes over used substrates involving a bath of sonicated acetone, a bath of sonicated isopropyl alcohol, rinsing with deionized water and drying with a nitrogen flow. After tests ensuring the cleanliness of the substrate, it was placed and centered on the chuck of the spin-coater. The sample was secured with vacuum and again cleaned with nitrogen gas flow just before applying the solution with a pipette onto the substrate. To evaluate the films, these were first coated onto silicon and glass substrates to measure properties as the thickness, composition through spectral analysis, and surface quality with optical microscopy. For electrical measurements, the films had to be sandwiched between conductive electrodes in order to make electrical testing of properties and for further design of the final devices.

The first batch of films were coated onto silicon wafers that were previously cleaned; thus the adhesion of the PVDF film over the surface of the wafer was nor compromised

by particles or residues. The wafers were spin coated with PVDF-TrFE from *PIEZOTECH* 10 %wt with 4 variations of spin-velocity and 3 variations of baking temperature. The parameters for speed were 1000, 2000, 3000, and 4000 RPM while the parameters selected for baking were 21, 80 and 135 degree Celsius. These values were selected in order to roughly check for best processing windows. After 3000 RPM the materials are expected to have reached the minimal thickness of the solution, 21 degrees Celsius is the cleanroom temperature (no bake) and 135 degree Celsius is a temperature just below the melting and Curie temperature of the material. 80 degree Celsius were chosen as an intermediate temperature to see process trends.

6.2. Thickness of cast films

Coated films were measured using initial scratch tests of the film using the *DekTak3ST* surface profilometer as a first measurement of the thickness of the spin-coated layer, the heights are illustrated in the table 6.1 shown below. These values are used as starting parameters for the more exact ellipsometric scans.

Speed RPM	Temp °C	Thickness μm
1000	21	4.0163
1000	80	3.8500
1000	135	4.0914
2000	21	3.3346
2000	80	2.9015
2000	135	3.1353
3000	21	2.1353
3000	80	1.9500
3000	135	1.9012
4000	21	2.1828
4000	80	1.8165
4000	135	1.8500

Table 6.1: Thicknesses of first batch

Ellipsometry was used to measure the thickness values more accurately than with the *DekTak* profilometer. The 200MM laser *Philips* ellipsometer available in the laboratory is capable of using three laser wavelengths for different measurement types and can calculate the thickness and refractive index (Ψ) indicating measured or expected values of the film thickness. Different measurements were performed using the three lasers of the ellipsometer to select for the future analysis, which one will perform the most precise measurements over the thin films.

Ellipsometry	LaserA	632 nm	
Speed\Temp	21	80	135
1000	4.062	4.063	4.067
2000	1.968	2.020	2.043
3000	1.950	1.980	1.984
4000	1.961	1.980	1.985

Table 6.2: Thicknesses of batch Ellipsometry Laser A

Ellipsometry	LaserB	1301 nm	
Speed\Temp	21	80	135
1000	4.080	4.133	4.047
2000	2.132	2.049	2.007
3000	2.173	1.739	1.620
4000	2.120	1.616	1.789

Table 6.3: Thicknesses of batch Ellipsometry Laser B

Ellipsometry	LaserC	1550 nm	
Speed\Temp	21	80	135
1000	3.994	4.245	4.154
2000	1.807	1.838	1.898
3000	2.275	1.749	1.687
4000	2.186	1.654	1.750

Table 6.4: Thicknesses of batch Ellipsometry Laser C

The ellipsometry from laser A seemed to be more consistent with the profilometry shown in table 6.1. The results from that wavelength were used for all further measurements of the films.

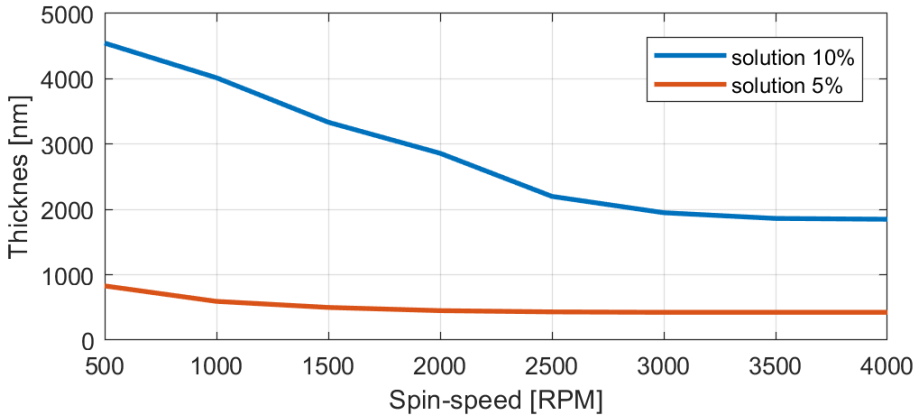

Figure 6.1: In this graph there are the thickness curves for PVDF-TrFE at 10 %wt and 5 %wt of dissolution

The thicknesses for PVDF-TrFE were measured for solutions of 10 %*wt* and 5 %*wt* and presented in spin-speed vs thickness curves, shown in figure 6.1. The curves show that the final thickness becomes stable (fixed) after 3000 RPM. Beyond thickness issues, the effect of spin-speed relation to the layers ferroelectric functionalities needs to be discussed in order to determine which would be the best conditions for the generation of a working transducer.

6.3. Effect of spin speed and temperature

In the images below the grain formation of the structure of PVDF under different spin-coat velocities and baking temperatures is shown. This baking is needed to immediately place the spin-coated sample at a certain temperature to evaporate residues of solvents and consolidate the future transducer layers. The images were taken from the Horiba Xplora Raman analyzer. These samples depict layers at three baking temperatures 135°C (below Curie temperature), 80°C (intermediate) and 21°C (room temperature) at the same spin-speed of 1500 RPM. The figure 6.2 shows the different crystal domains in the spin coated and baked layer with visible cells boundaries and without gap between grains. This is an example of a morphologically good layer of PVDF. The sample that was let to dry at room temperature, shown in figure 6.4 (21°C), shows dispersed grains, randomly spread over the surface of the substrate. The surface already indicates, that this layer shall not function properly. Finally, the substrate shown in figure 6.3 (80°C) shows bigger grains and a knit together structures. From this set of images it can be concluded that baking at 135°C, slightly below the melting point and Curie temperature, generates films with minimal pore formation and continuous surface; a good start for functional transducer layers.

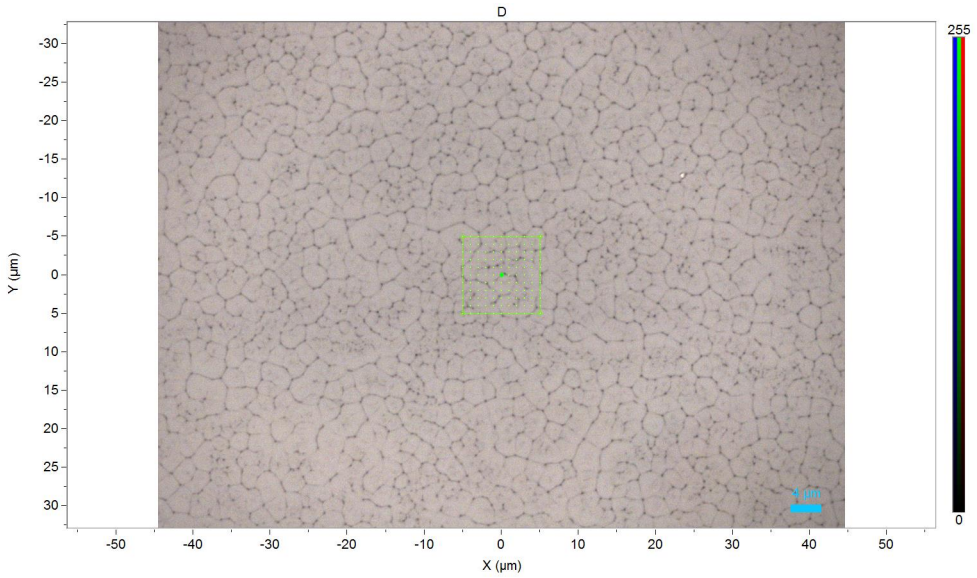

Figure 6.2: Surface from thin film made of PVDF at 1500RPM 135°C 100x it is possible to see the grain domains all joined together, the constituting grains seem to be bigger than in the other samples

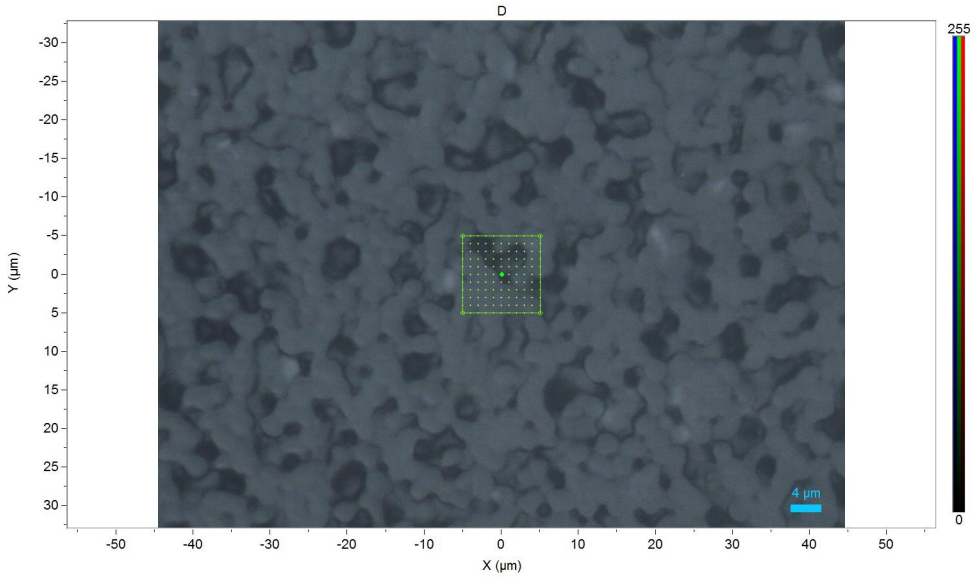

Figure 6.3: Surface from thin film made of PVDF at 1500RPM 80°C 100x it is possible to observe the grains join together, the film may be porous

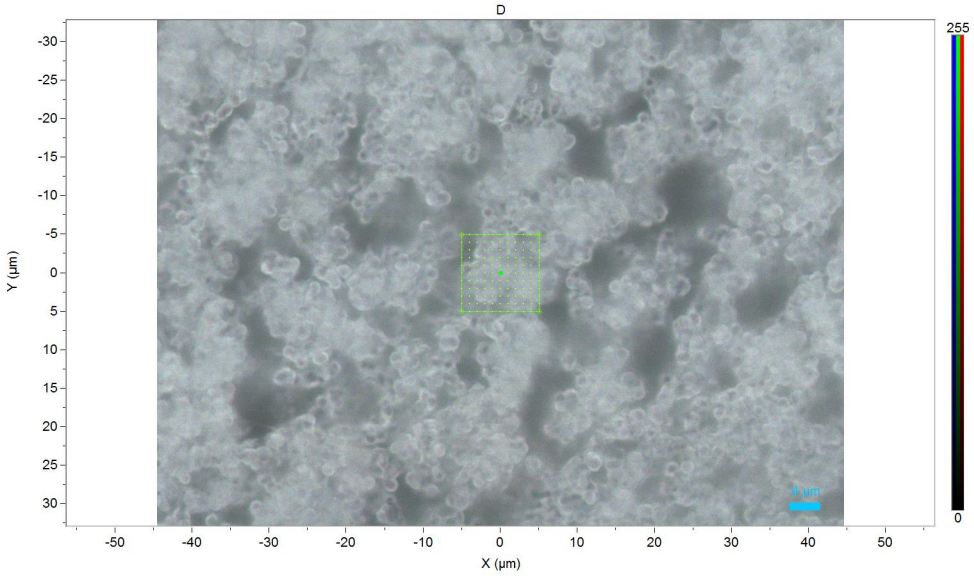

Figure 6.4: Surface from thin film made of PVDF at 1500RPM 21°C 100x it is possible to appreciate a non-continuous surface with non connected grains, the material is not suitable for further use

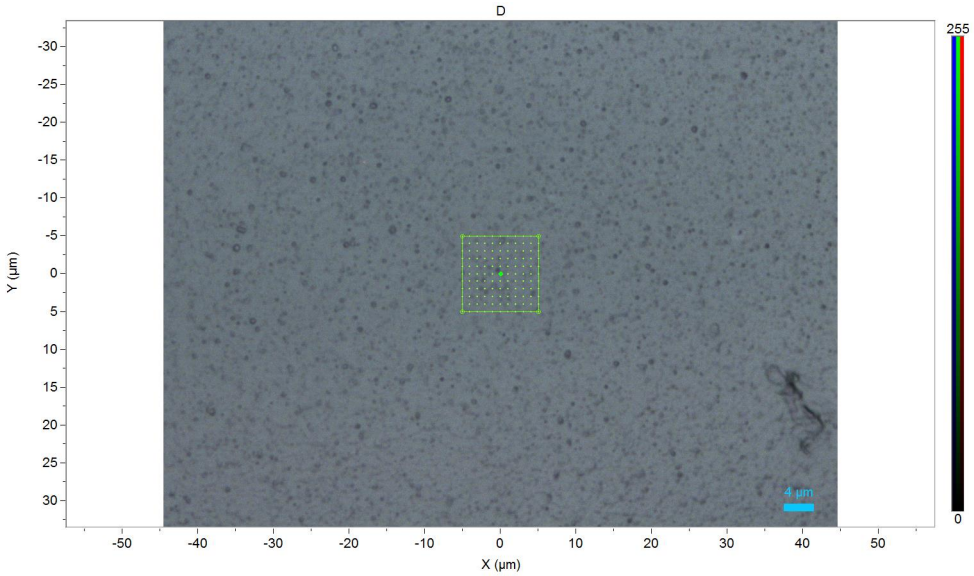

Figure 6.5: Surface from thin film made of PVDF-TrFE at 1500RPM 80°C 50x it is possible to see a continuous surface with a small quantity of porosity

In figures 6.5 and 6.6 samples baked at 80° Celsius, and spin-coated at 1500 and 2500 there was no appreciable change in the surface, which results to be homogeneous.

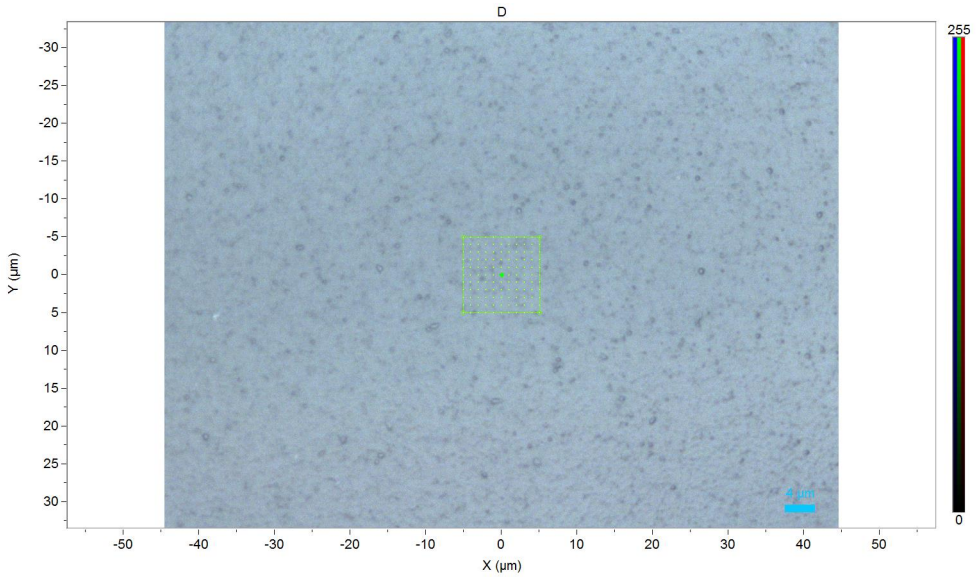

Figure 6.6: Surface from thin film made of PVDF-TrFE at 2500RPM 80°C 50x it is possible to appreciate a continuous surface over the shown area

So far the observation is, that coating at low spinning speeds may guarantee high thicknesses, yet the surface of the material seems to be very porous if it is not baked immediately after the coating process as shown in figure 6.4. This problem is fixed, when the PVDF is immediately baked at temperatures slightly below the melting point as shown in figure 6.2. When coating PVDF-TrFE, the baking doesn't really compromise the surface of the layer due to the low boiling point of the solvents used for the prepared solution. The homogeneity of the films is shown in figure 6.5 and figure 6.6. In order get the best layers it is recommended to spin-coat the samples at speeds above 2500 RPM and immediately bake them at 135° Celsius, to evaporate all the solvents, reduce porosity and consolidate the grains of the semi-crystalline matrix of the polymer. To confirm these assumptions Raman spectroscopy is used to measure the ferroelectric capabilities of the coated films.

6.4. Raman spectroscopy

Raman spectroscopy is a spectral analysis method capable to analyze the composition and properties of materials as explained in the previous sections. Here, the most important spectral bands describing the phase composition of the material can be analyzed in a comparison of the relative peak size between the $\alpha-$phase ($794cm^{-1}$) and the desired $\beta-$phase ($840cm^{-1}$). This indicates which process conditions favor the domain of the required ferroelectric $\beta-$phase.

A set of samples was coated onto silicate substrates, due to the reduced spectroscopic interference of the substrate for analysis, at 1500, 2500 and 6000 RPM and immediately baked at 21°C, 80°C and 135°C, the higher speed was selected to show if there was an influence by speeding up the drying process.

The graphs are displayed in a specific order of velocity variation and fixed temperature 21°C, (figure 6.7) and 135°C (figure 6.8), and, on the other side, organized

by temperature variation with fixed velocity at 1500 RPM (figure 6.9) and 6000 RPM (figure 6.10). Thus the influence of the different parameters can be seen in direct comparison. All the presented graphs are normalized to the highest peak values.

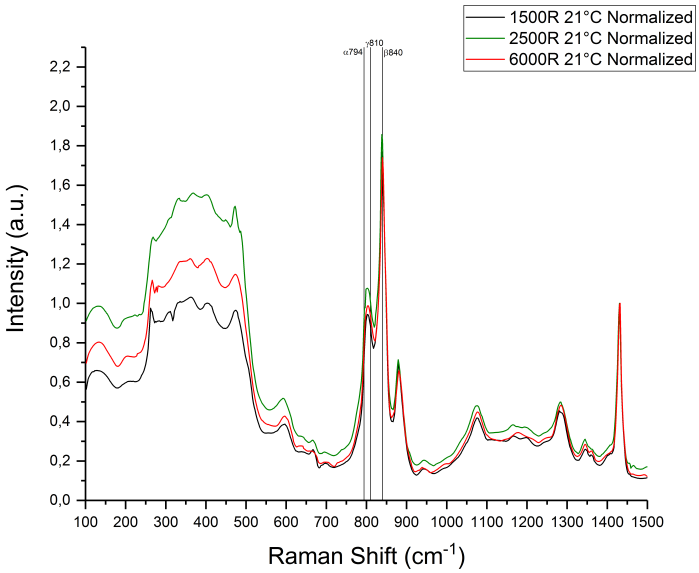

Figure 6.7: Raman spectroscopy of samples made from PVDF-TrFE coated at 21 degrees Celsius baking, evidence, that the change in spin-coating velocity doesn't significantly change the relative peak height between α and β peaks

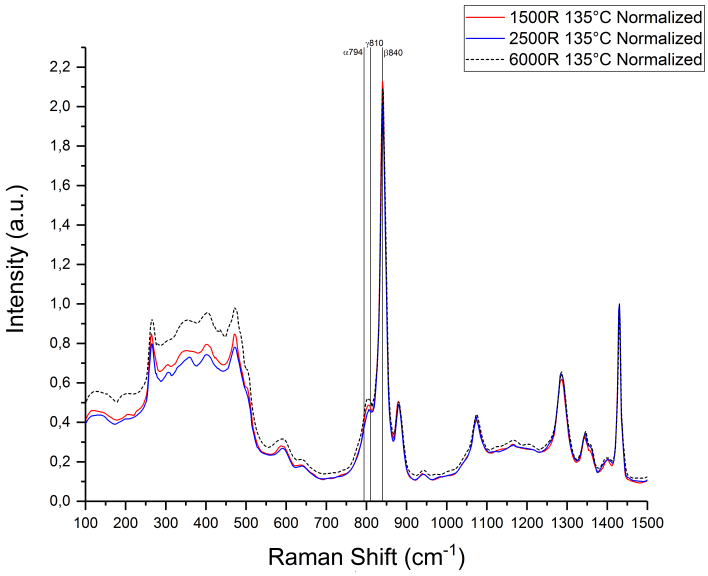

Figure 6.8: Raman spectroscopy at samples made from PVDF-TrFE cast at 135 degrees Celsius baking, the change in spin-coating velocity doesn't change significantly the relative distance between α and β peaks

From figure 6.7 and figure 6.8, it is clear, that the change in spin-coating velocity doesn't really affect the relative amount of *beta* and *alpha* phase. A change in the ratio of the phases can be observed in figure 6.8 indicating, that the α peak has almost disappeared. Here temperature seems to have an influence when comparing the parameters between figure 6.7 and figure 6.8.

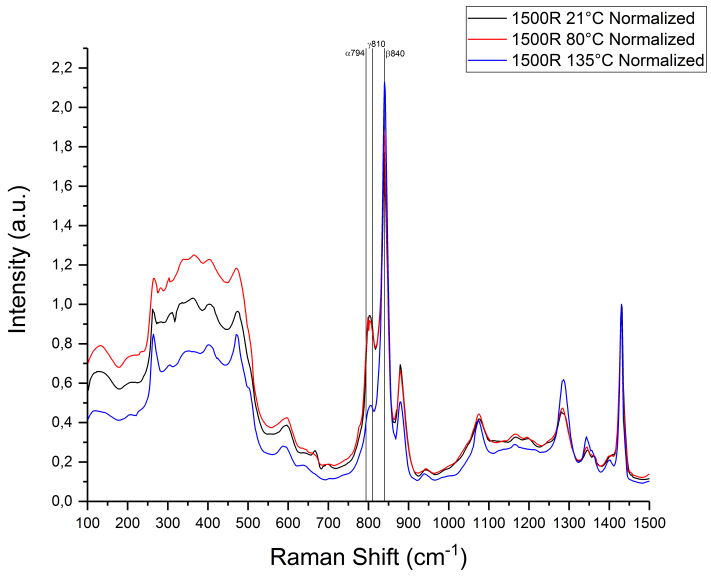

Figure 6.9: Raman spectroscopy at samples made from PVDF-TrFE cast at 1500 RPM spun sample, the change in baking temperature affects the samples

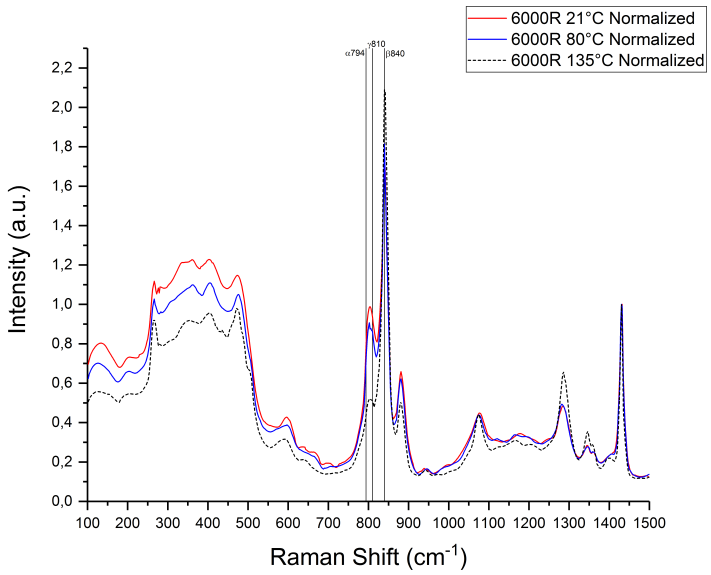

Figure 6.10: Raman spectroscopy at samples made from PVDF-TrFE cast at 6000 RPM spun sample, the change in baking temperature affects the samples

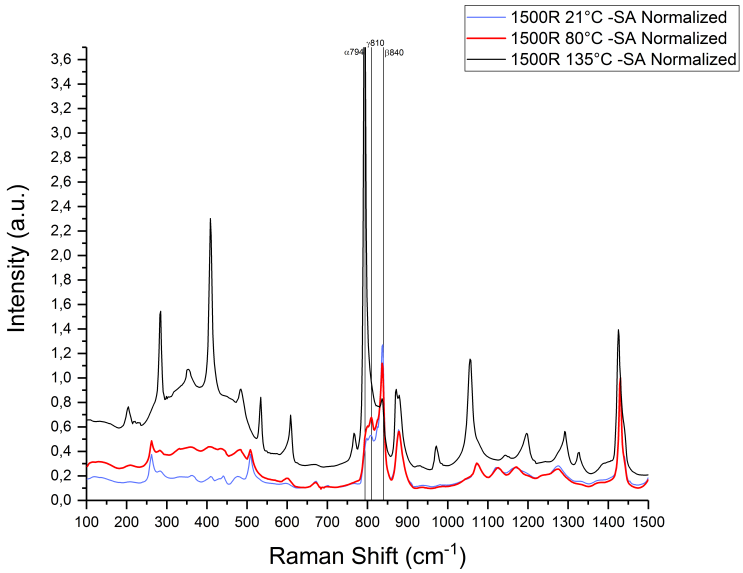

Figure 6.11: Raman spectroscopy at 1500RPM spun sample Sigma-Aldrich, $alpha-$phase is increased with the increase of baking temperature

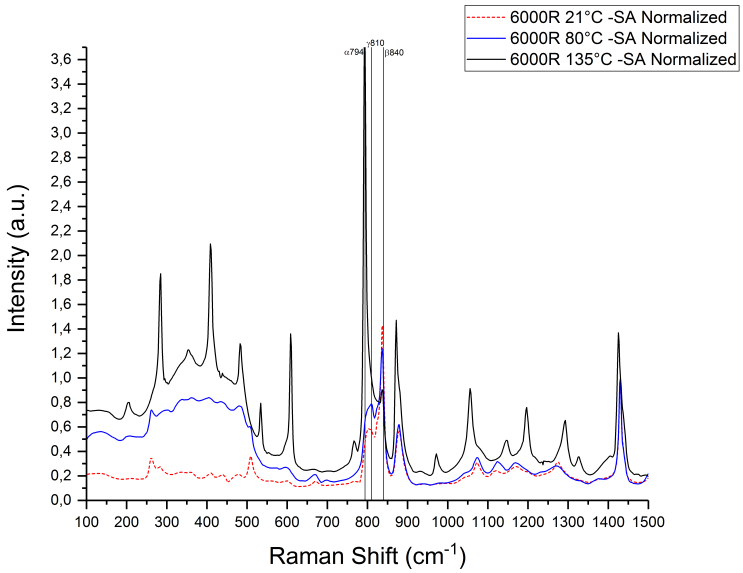

Figure 6.12: Raman spectroscopy at 6000RPM spun sample Sigma-Aldrich, $alpha-$phase is increased with the increase of baking temperature

It is shown in figures 6.9, 6.10, 6.7 and 6.8, that the relative height between the 794 cm^{-1}, related to the non-ferroelectric phase of PVDF, and the 840 cm^{-1}, related to the active ferroelectric phase, is strongly dependent on the elevated baking temperature of 135° C. Here the image shows a major fraction of $\beta-$PVDF against the undesired $\alpha-$PVDF phase. On the other hand, the changes between different spin-speeds shown in the graphs do not contribute significantly to the ratio between $\beta-$PVDF and $\alpha-$PVDF.

Further, the standard pure PVDF (Sigma-Aldrich), shown in figure 6.11 and figure 6.12, shows a minimal ratio of $\beta-$PVDF against $\alpha-$PVDF, which means, that in case of further processing the PVDF won't have a high piezoelectric response. From this spectral analysis it can be concluded, that inclusions of copolymer and high baking-annealing temperatures are the dominant factors to achieve high quantities of β active PVDF. For the following process steps, the baking temperatures of the samples were set to 135°C with spin coating speeds above 2500 RPM which will further improve the film homogeneity in the samples. These process conditions and layer qualities build the first set of parameters used to implement a lithographic process with a functional PVDF layer.

6.5. Lithography performed with PVDF

In order to explore the capabilities of processing PVDF by standard methods available in the facilities, samples with layers of PVDF-TrFE were spin coated with AZ5214E photoresist. The resist was spin-coated using the standard parameters, spinning the material at 4500 RPM for 30 seconds and baking the resist at 115°C for 30 seconds. Optical morphological inspection indicated, that the layer of PVDF under the AZ5214E layer was unaffected by the process. Thus the PVDF-layer was not diluted by the AZ5214E solvent.

The resist covered samples were exposed to UV-light under a thin foil shadow mask with big squared patterns. These patterns were developed with AZ standard developer, dipping the samples for 7 seconds under developer and subsequently eliminating the residues of the developer by immediate rinsing with deionized water followed by drying with a nitrogen pistol.

The image below shows the PVDF with patterned resist at different magnifications. The major defects are assumed to be caused by thin foil lithography mask technique and due to light propagation effects during exposure. The lower right image shows the PVDF patterning under the elaborated mask after being treated by oxygen plasma etching. With adaptations in handling of the process steps, PVDF can be used with standard lithographic methods. Possible effect due to etching will be shown in the SEM lithography inspection section of this manuscript.

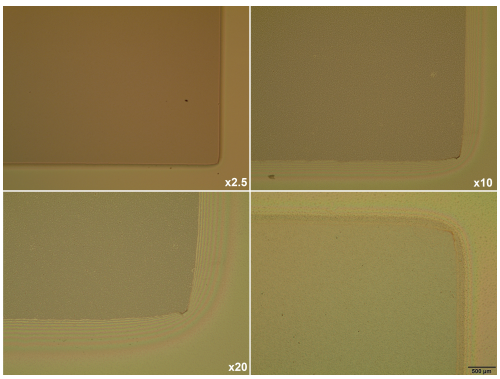

Figure 6.13: PVDF processing at different magnifications, last image (lower right) represents masked PVDF-TrFE treated with oxygen plasma

6.6. Electroding of thin films

To characterize the piezoelectric and dielectric properties of the material, a design was layed-out, to fabricate a set of capacitors. The devices were fabricated in the following way: The substrate was a 600 μm silicon wafer that was previously cleaned in a bath of acetone and isopropyl alcohol, followed by rinsing with DI water and dried with nitrogen to eliminate any possible remaining impurities. Next, a 200 nm layer of aluminum was evaporated onto the wafer to generate the bottom contact. Then a layer of $2\mu m$ of PVDF-TrFE was spin coated on top of the aluminum layer. The wafer was baked at 135° Celsius for 1 hour to evaporate any remaining solvent of the polymer and to achieve improved ferroelectric behavior. Afterwards a shadow mask process for sputtering was used to evaporate the upper electrode pattern composed of another 200nm layer of aluminum. The shadow mask process is illustrated in figure 6.16 (left side).

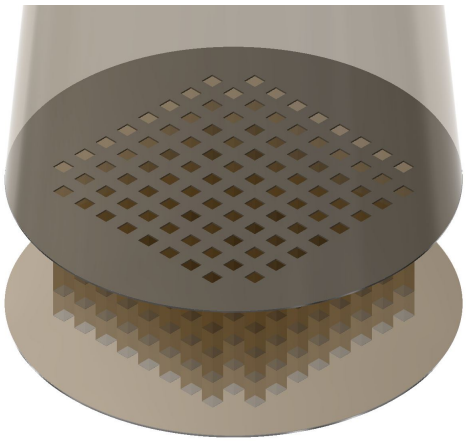

Figure 6.14: Evaporation process with shadow mask

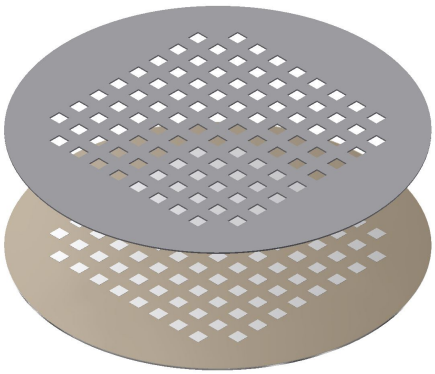

Figure 6.15: After sputtering the top electrodes, a matrix of PVDF capacitors is left over the substrate

Figure 6.16: Fabrication process through shadow masked sputtering (left) and fabrication process through photolithographic method (right)

A second process type, more suited for higher resolution transducers, was also tested and is shown in figure 6.16 (right). This process is started with a sputtered bottom $200nm$ aluminum electrode, followed by a spin-coated layer of PVDF, an upper electrode from a $200nm$ aluminum layer. The resist used to pattern the upper electrode was AZ1452E which can perform as either positive or negative resist. The patterning of the electrodes was performed with a mask pattern featuring circles of different diameters from $100\mu m$ to $350\mu m$. The spin-coated layer of AZ resist was exposed with UV light, developed and tested with wet and dry etching procedures. The wet etching was performed with phosphoric acid (Aluminum Etchant from MicroChemicals) while the dry etching was performed using chlorine plasma chemistry BCl_3.

6.7. SEM lithography inspection

The devices were inspected by SEM imaging. The images below depict samples of PVDF coated using a spin velocity of 3000 RPM and 4500 RPM, with 200nm thick electrodes. For these devices glass substrates were used.

Some samples were broken in order to inspect cross sections in SEM in detail. In the first images it is possible to see the patterning of the round electrodes on the sample surface. The different layers in the cross section show the capacitor structure in figure 6.17. The thickness of the PVDF solution ($10\,\%wt$) between 1200 and 1800 nanometer can be seen, showing a uniform layer with only small variations in the material thickness. In figure 6.19 the circular pattern with circular electrodes with corresponding sizes of 100, 150, 250 and 350 μm can be seen. The cross section method was also used to identify plasma etching behavior of the PVDF. Here, another set of samples was etched in a barrel reactor with oxygen plasma with a flow rate of 900 ml/min. The AZ5214E photoresist on top, was used as mask for the PVDF layer. After 120 seconds of plasma etching, the PVDF was etched through down to the bottom electrode, yet the isotropic etching behavior of the barrel reactor shows drastic underetching results.

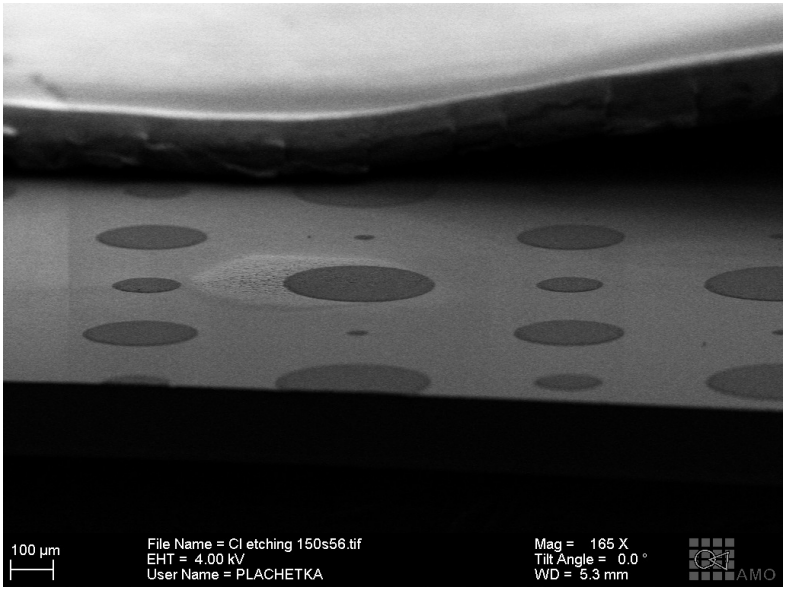

Figure 6.17: Patterning of aluminum film through chlorine chemistry

This capacitor structure will likely fail due to arcing, since only air is between the electrodes on the outer rim of the device. Part of the layer of AZ5214E still remains as mask on the upper aluminum electrode.

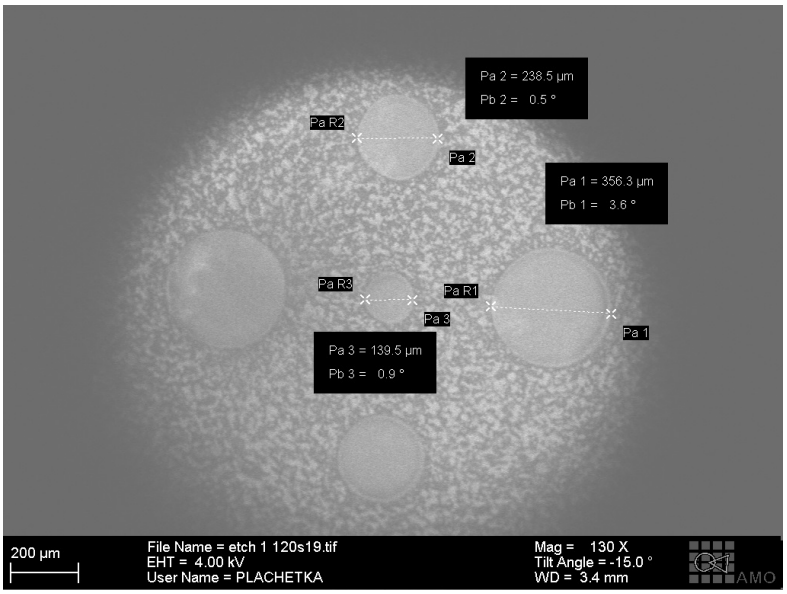

Figure 6.19: Top view patterning of aluminum film through chlorine chemistry

In figure 6.18 the cross-section of one of the capacitors which has been patterned by chlorine chemistry can be seen. The resist (rugged surface) on top of the aluminum layer on top of the thin (200 nm) aluminum layer and the etched structure can be seen. The top in figure 6.19, the detail of the PVDF surrounding the electrodes is visible.

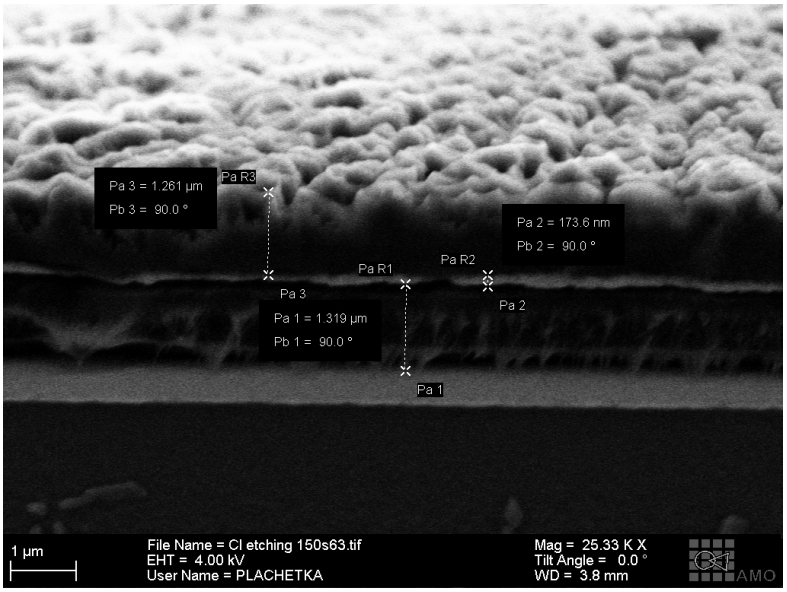

Figure 6.18: Cross section patterning of aluminum film through chlorine chemistry

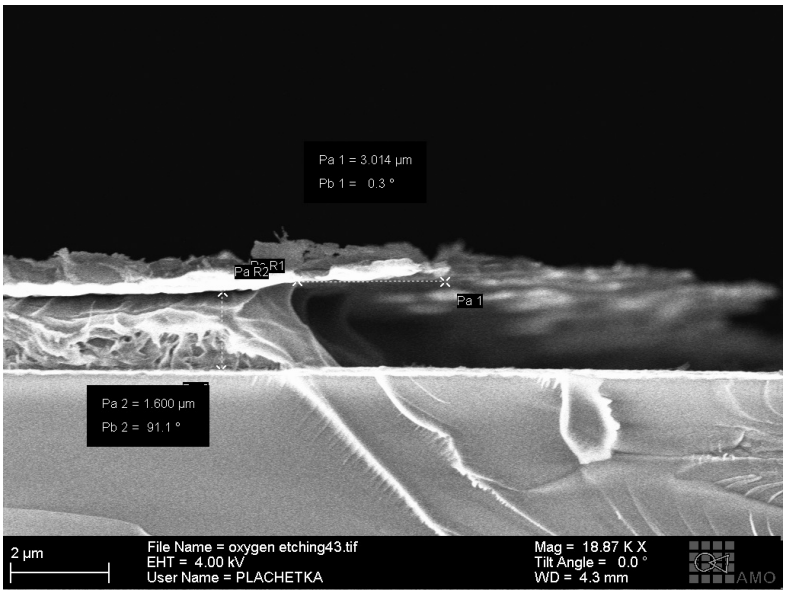

Figure 6.20: Etching of PVDF through oxygen etching

This problem might be compensated when using a more sophisticated RIE (reactive ion etching) machine. Though these were only temporarily functional at the facility due to gas connections made to another machine. The rest of the PVDF was completely removed from the bottom electrode, showing that the whole composition of PVDF-material matrix can be removed with oxygen plasma only, according to figure 6.20. Also, part of the layer of AZ5214E still over the aluminum layer, this could be removed after with acetone. These samples were sent to *Radiant Technologies inc.* in the United States for further tests on poling and characterization.

6.8. Hysteresis measurement setup

In order to check the effectiveness of the processes and to evaluate the material for its ferroelectric capabilities, it is necessary to go beyond Raman spectroscopy and correlate the structure of the material with the electrical properties. For these devices it is possible to do a simple but effective electrical characterization using a custom electrical board which is capable to obtain the hysteresis windows characteristics of the ferro-electric materials. This custom board was planned to measure bigger samples with electrodes of 5mm as shown in the appendix A. The custom board is slightly based on the original Sawyer-Tower (S-T) circuit, which has demonstrated its use for very practical characterization of ferro-electrics and also to study fundamental phenomena such as spontaneous polarization, remnant polarization, coercive-field, and polarization reversal mechanisms. The basic Sawyer-Tower circuit is useful for materials, which have a low loss and high polarization.
The custom board was made with the following schematics. Its function principle is to apply a sinusoidal waveform to the device under test (DUT), measure the voltage in the capacitor through a subtract circuit and to get the charge of the DUT through the integral of time of the current flowing through the capacitor. The circuit artwork was designed with the help of PCBwizard editor transferred and fabricated through copper etching techniques over a phenolic plate with the individual components soldered manually.

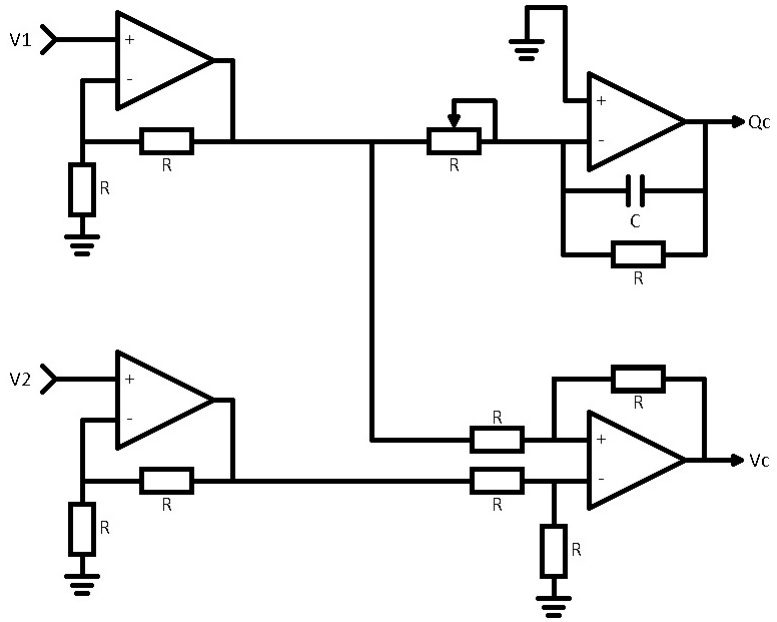

Figure 6.21: The circuit takes $V1$ and $V2$ from figure 6.22, the configuration measures the voltage of the capacitor Vc and integrates the current of the capacitor to obtain the charge Qc

The circuit design was operated by means of a function generator integrated in an oscilloscope (MDO-2104EX). The current measurements presented in the images below were performed at a frequency of 1000 Hz, with a sinusoidal excitation waveform with

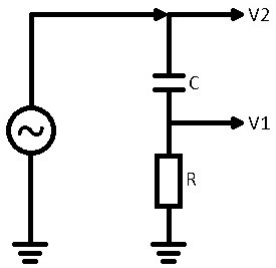

Figure 6.22: Measuring setup for voltage and current, the voltage received by the capacitor C is measured between $V1$ and $V2$. The current of the capacitor C is measured by the resistor R

an amplitude of 5 volts. The physical measurement setup is illustrated in figure 6.23. The measuring circuit is connected to a symmetrical power supply through plug connectors and the signals that go outside (excitation) and inside (input) the oscilloscope are connected through BNC cables. Control of the measurement and data acquisition is performed with a computer connected to the oscilloscope with LabView. The samples are connected through custom sample holders as in figures 6.24 and 6.25. After connecting the equipment and setting the samples into position, the terminal in LabView was set to the excitation signal of the integrated waveform generator. It captured the data and displayed it on the computer screen with the data stored for the purpose to be post-processed in other software as Matlab. The terminal is shown in figure 6.26.

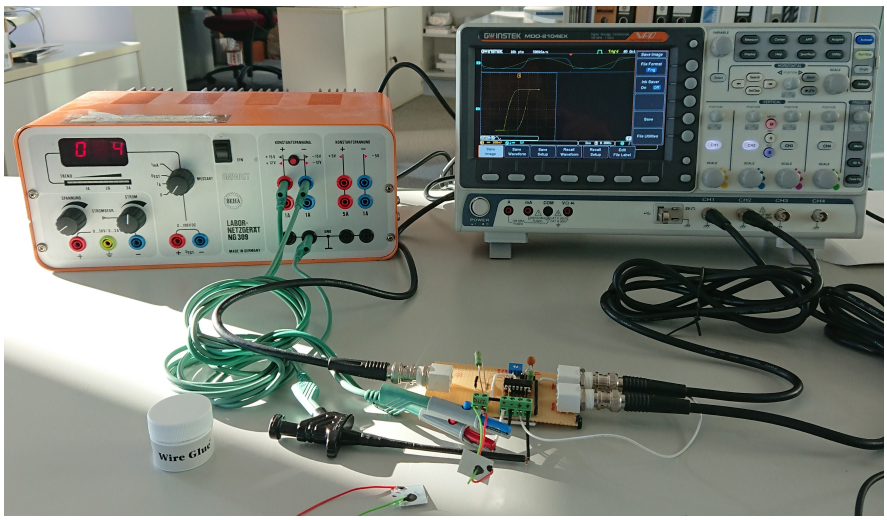

Figure 6.23: Physical measuring setup

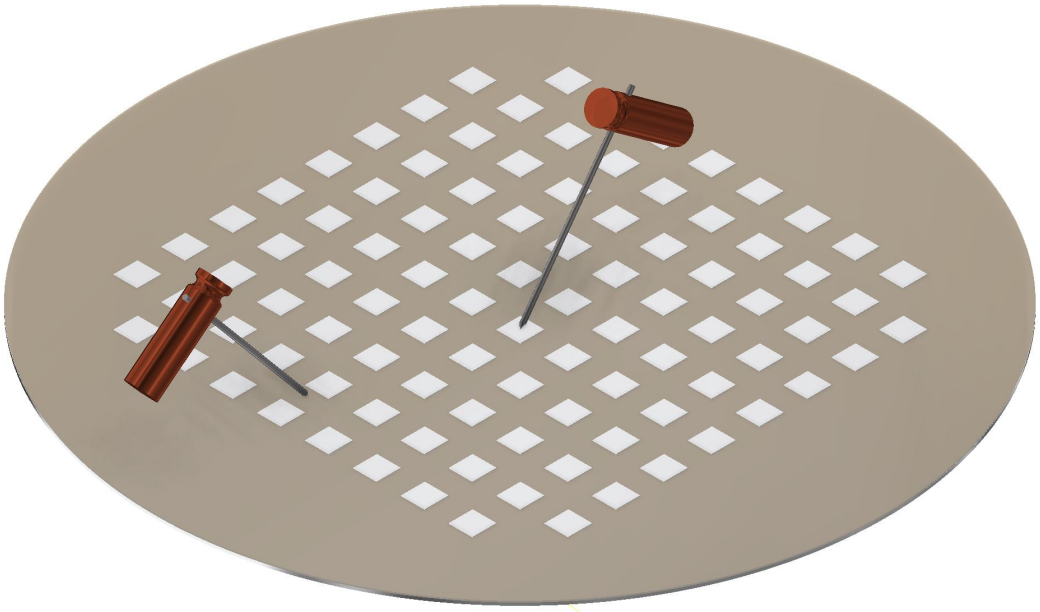

Figure 6.24: The fabricated devices can be tested and measured with the help of a probe station, the tips can be easily adjusted and connected to available measurement devices as an impedance meter

Figure 6.25: The image shows the probes getting in contact with the metal conductive pads of the fabricated capacitors created over the surface of a wafer

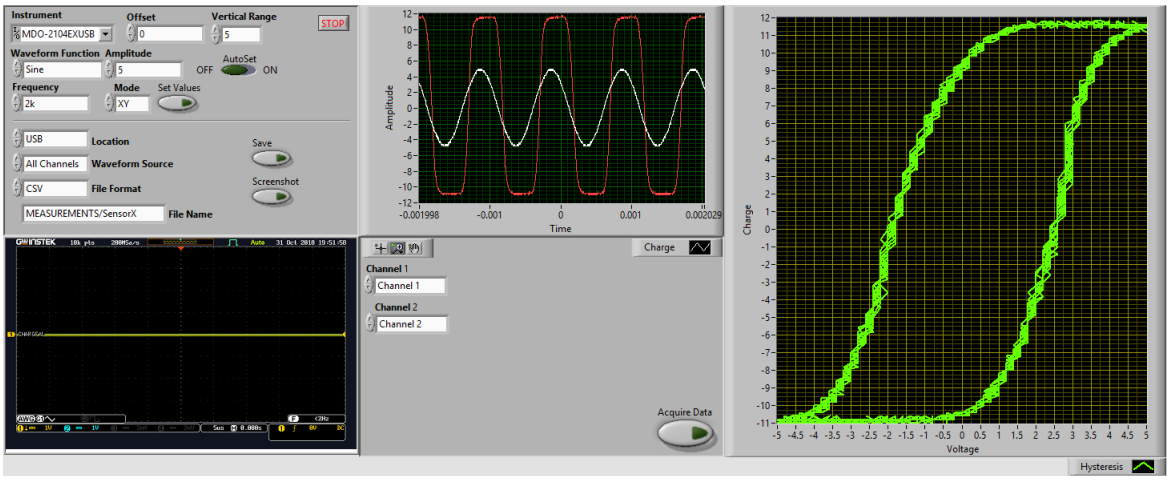

Figure 6.26: Terminal of LabView program designed to acquire electrical data and drive hysteretic analysis, using oscilloscope MDO-2104EX

The graph 6.27 shows the hysteresis loop of a sample that was fabricated in the laboratory under coating speed of 3000RPM and baking temperature of 135°C with PVDF-TrFE from PIEZOTECH. The graph 6.27 shows the hysteresis loop of a sample that was also fabricated in the laboratory under same conditions (3000RPM, 135°C) with the only difference that the processed material was pure PVDF from Sigma-Aldrich.

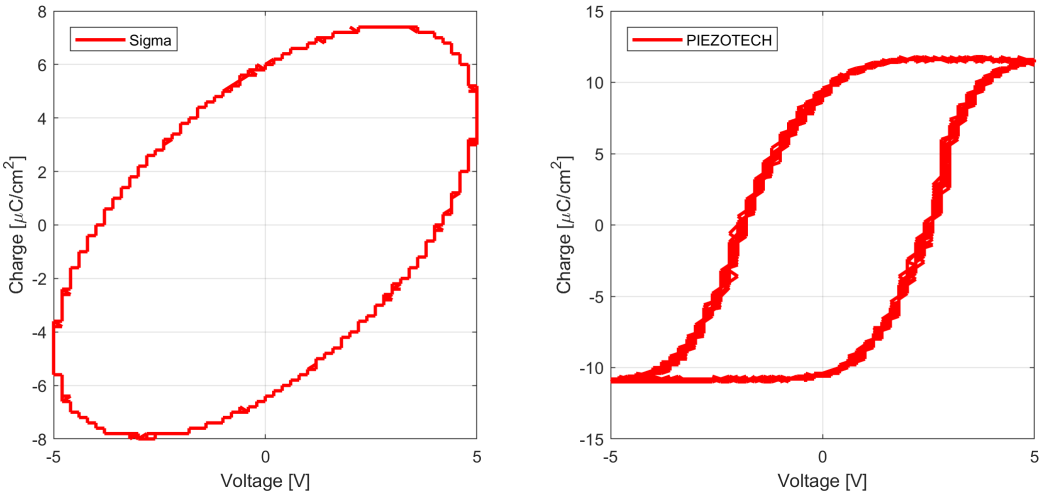

Figure 6.27: Ferroelectric curve for device fabricated at 3000RPM 135°C, the image presents the ferroelecric hysteresis loop for the PIEZOTECH PVDF-TrFE, the hysteresis loop didn't occur for the pure PVDF from Sigma-Aldrich

The graphs presented on figure 6.27 show the difference between a ferroelectric and a non-ferroelectric material. Measurements were performed with the self-built board and test sequence described earlier. The material from pure PVDF (Sigma Aldrich) shows the behavior of a lossy capacitor, which means that charge will be build up proportional

in the direction of the change of voltage with deviations only caused by the resistive loss. On the other hand, using the PVDF-TrFE there are limits as the coercive field or voltage. This is the value of voltage that needs to be applied to the material in order to cause a reversal in the polarization which is expressed as the quantity of charge per unit of area and the remnant polarization which is the polarization level of the material when no field or voltage is applied to it. Higher polarization levels and low coercive fields specify how easy the material can be polarized and changed in its physical state. Samples made by photolithography were sent to *Radiant Technologies inc.* for the analysis of electrical properties and hysteresis. Similar to these samples presented in *SEM lithography inspection* section, samples with different fabrication parameters were sent in order to observe if there was a noticeable difference between fabrication parameters. There were two series of samples the *A-series* consists of devices coated over glass substrates in the shape of squares of 20 by 20 cm and the *B-series* consists of devices coated over borofloat 4 inch wafers.

	Pmax($\mu C/cm^2$)	Pr($\mu C/cm^2$)	-Pr($\mu C/cm^2$)	V_c	$-V_c$	$C_{(Max-Eff)}(nF)$	κ(Eff)
A1	5.540	4.439	-4.451	78.769	-76.448	0.021	25.053
A2	6.025	5.239	-5.266	74.560	-73.185	0.023	27.245
A5	4.352	3.525	-3.531	80.431	-78.682	0.017	19.681
A6	5.246	4.380	-4.402	82.037	-80.325	2.623	23.725
A7	5.238	4.163	-4.201	81.105	-79.431	0.020	23.688
A10	5.678	5.023	-4.959	88.132	-79.205	0.022	25.677
B1	10.973	9.378	-9.383	47.612	-44.115	0.042	49.621
B2	12.866	11.242	-11.208	42.273	-39.254	0.050	58.181

Table 6.5: Ferroelectric measurement results

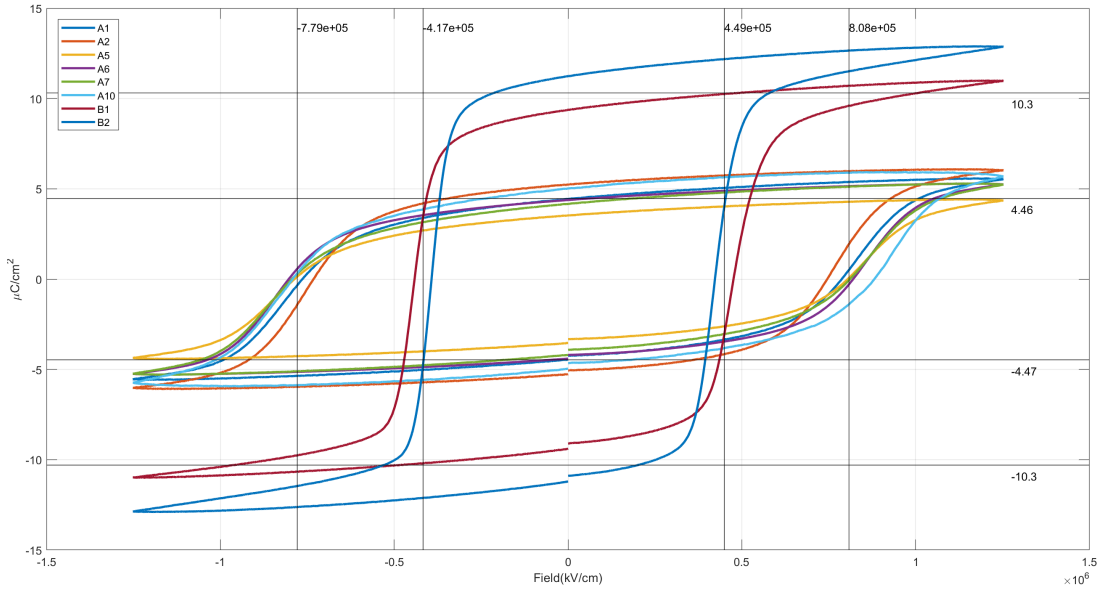

Figure 6.28: Ferroelectric measurements made over samples made of PVDF-TrFE from PIEZOTECH, the lines indicate the mean coercive field and the mean Remnant polarization

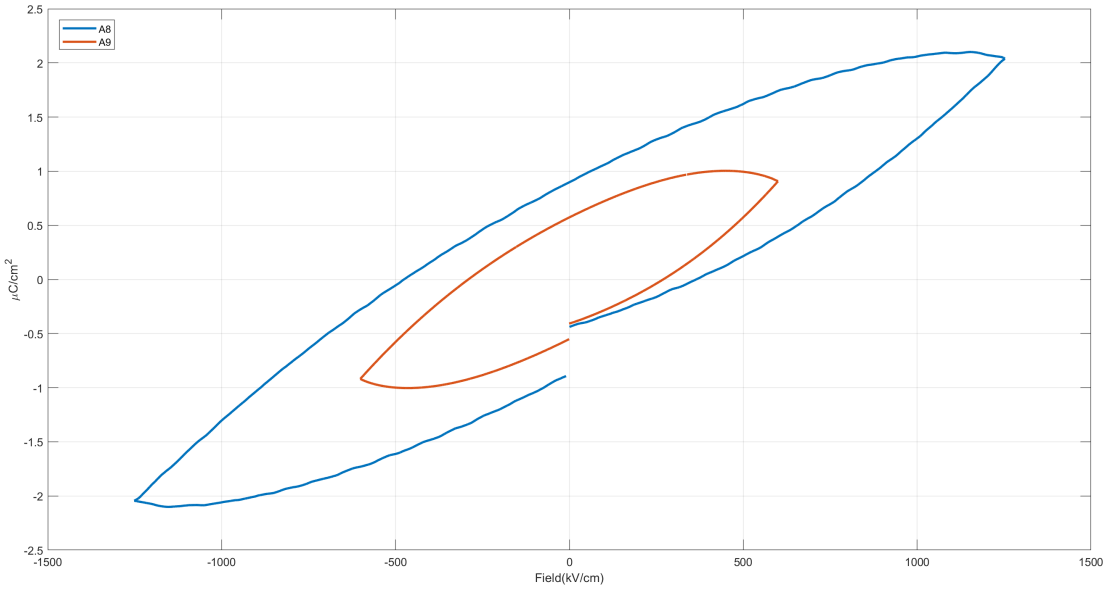

Figure 6.29: Ferroelectric measurements for samples made from Sigma Aldrich PVDF, the lack of a hysteresis loop is shown in the graph

The measurements performed by Radiant show the same behavior as the ones analyzed by the equipment developed during this master thesis. From figures 6.27 to 6.29 the differences between PIEZOTECH (PVDF-TrFE) and Sigma-Aldrich (PVDF) are visible. There is no relevant coercive field limit in figure 6.29 nor a remnant polarization level. This material does not show a ferroelectric functionality as could already be predicted by the Raman spectroscopy measurement. Here the material showed almost a nonexistent fraction of $\beta-$phase against the non-electroactive $\alpha-$ phase. In contrast the PVDF-TrFE from PIEZOTECH shows a clear hysteresis curve, evidencing its ferroelectric functionality, as was anticipated already during the Raman measurements.

The table 6.6 describes the samples sent to *Radiant Technologies inc.* and the processes used to elaborate the samples. These *A series* were processed on glass substrates of 20 by 20 mm, while the *B series* were coated onto complete 4 inch borofloat wafers. The results of Radiant show that the *A series* have an average coercive voltage (V_c) of 80.84 $Volts$ positive and -77.88 $Volts$, and an average remnant polarization (P_c) of 4.46 $\mu C/cm^2$ positive and -4.47 $\mu C/cm^2$ negative. The *B series*, had an average coercive voltage (V_c) of 44.94 $Volts$ positive and -41.69 $Volts$ with an average remnant polarization (P_c) of 10.31 $\mu C/cm^2$ positive and -10.30 $\mu C/cm^2$ negative.

Name	Size	Spin-Speed	Annealing	Etching	Strip	Material
B1	4in	3000	135°	wet	Acetone	PIEZOTECH
B2	4in	4500	135°	dry	Acetone	PIEZOTECH
A1	2x2	2500	135°	wet	Acetone	PIEZOTECH
A2	2x2	3000	135°	wet	Acetone	PIEZOTECH
A3	2x2	2500	135°	sputtered	XXX	PIEZOTECH
A4	2x2	3000	135°	sputtered	Acetone	PIEZOTECH
A5	2x2	4500	135°	dry	Acetone	PIEZOTECH
A6	2x2	4500	135°	sputtered	Acetone	PIEZOTECH
A7	2x2	4500	135°	dry	DMSO	PIEZOTECH
A8	2x2	3000	135°	dry	Acetone	ALDRICH
A9	2x2	3000	135°	dry	XXX	ALDRICH
A10	2x2	3000	135°	dry	Acetone	PIEZOTECH

Table 6.6: Description of samples sent to Radiant Technologies with fabrication parameters

6.9. Discussion of electrical Results

In order to interpret which parameters could have affected the electrical and electromechanical behavior of the devices, a small calculation has been made to show how the active area and thickness of the device could favor these properties.

For the calculation of the capacitance, the following quantity is expected according to the formula.

$$C = \epsilon_0 \epsilon_r \left(\frac{A}{d} \right) \tag{6.1}$$

Where:
ϵ_0 is $8{,}854 \times 10^{-12}$ F/m
ϵ_r is $10 - 12$
A is the area of the electrode and
d is the distance between electrodes

The effective expected capacitance is represented in two graphs in which the way the capacitance should vary, depending on the thickness and the area of the device, is illustrated. The first graph represents the capacitance when varying the active area of the capacitor at a thickness of 1.5 μm and the second graph represents the capacitance on a fixed active area of 1 mm^2. It can be seen that the thickness favors higher capacitance of the devices while a change in the active area has less influence.

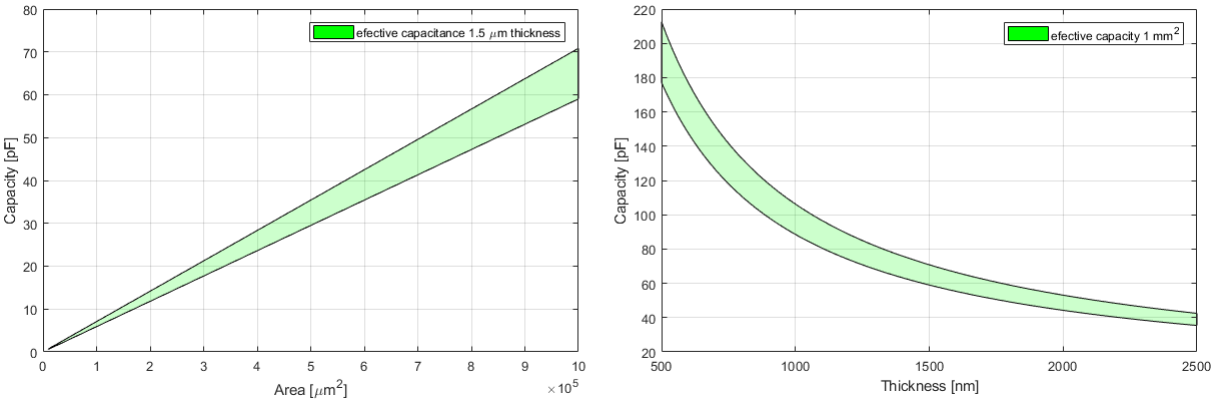

Figure 6.30: Capacitance effective area

The field expressed in the graphs highly depends on the fabrication methods used to process the material. The value of the relative dielectric constant of the material can change due to the previously mentioned handling and fabrication conditions.

For the first calculation of the displacement-voltage relationship generated by the device, it is necessary to consider the following equation.

$$\Delta L = d_{3i} \left(\frac{V}{t} \right) L \tag{6.2}$$

Where:
ΔL is the change of longitude of the material
d_{3i} is the piezoelectric constant $d_{33} = (-30) - (-24) pC/N$
V is the applied voltage and
t and L are the distance between electrodes

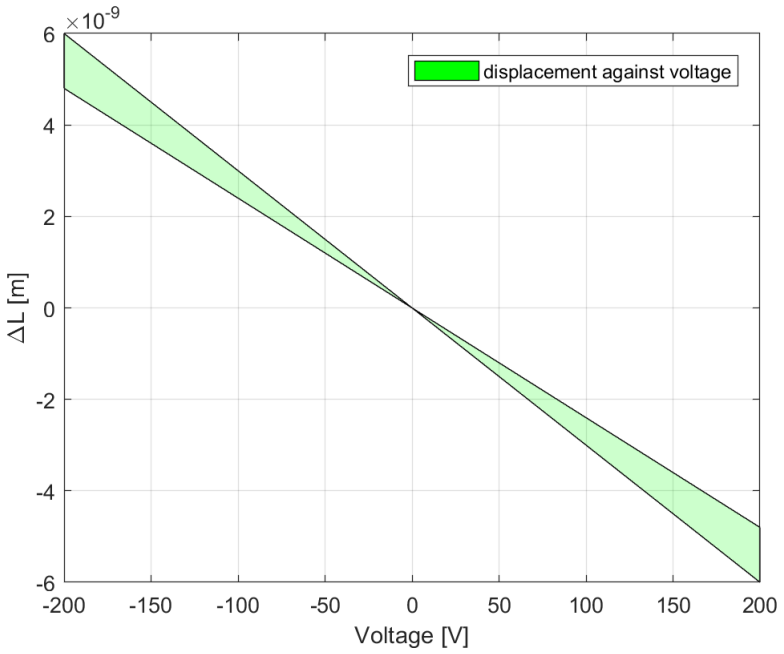

Figure 6.31: Piezo deformation against voltage

For the electrical response of the material, it is shown that the thinner the material the higher is the electrical field (V/t) obtained. Thus, for an actuator, the higher the electrical field, the more ratio of deformation ca be obtained. Yet, since the distance L and the thickness t have the same value for this kind of device, the displacement is only dependent on the applied voltage. Consequently, the major advantage of thinning the device is, that the driving voltages can be reduced, eliminating the necessity of complex electronics to drive actuators based on this kind of concept. The same rules apply for the application of a similar device concept as a sensor for detection of deformation. Here, other necessities can impose tighter specifications, that make thinning of the PVDF-layer reasonable. For example, the application of the PVDF-layer for detecting deformation of a foil like membrane or thin plastic foil. It is trivial, that the sensing PVDF-layer should be much thinner than the foil itself or the sensor layer would drastically influence the performance of the test subject. For both types of transducers, sensor and actuator, another factor limits the layer thickness. For a functional poling of the PVDF, described in the early sections of the manuscript, a higher material thickness will also need a higher poling voltage. For comparison of the devices fabricated with lithography and shown in the SEM section, the average capacitance calculated according to formula 6.1 was 0.0218 nF which is really close to the average of the capacitance measurements performed by Radiant of 0.0206 nF considering measurements over 350 μm radius electrodes. From the Radiant measurements, the effective κ was of 24.178, these values are extracted from table 6.5.

6.10. Poling results, process and variables

In order to make the PVDF electromechanically active, it is necessary to align the single regime polarities with a poling method. For the poling performed for this thesis,

a procedure had to be developed using equipment at AMO. The trials for the poling were first performed on thin glass samples in order to explore the best way to apply the procedure.

The PVDF-samples fabricated on glass at 3000 RPM and 135°C were placed onto a plate with probes connected to a *Keithley 2400* sourcemeter. The device is capable of delivering up to 200 volts and measure current and voltage, making the polarization current visible during the poling process. The source meter itself is not capable of performing a proper polarization cycle, thus it was necessary to elaborate a *LabView* program capable of applying the required waveform at the desired amplitude and frequency.

For the poling the Bauer method is used [17]. In his patent Bauer depicted the way to polarize ferroelectric materials in a replicable and homogeneous way, through the application of an electric field E to these materials. The material should be subjected to an alternating electric field E, at a frequency from about 0.001 to 1 Hz. The frequency is to increase gradually and in a cyclic way between $\pm 0 E_N$, where E_N should be slightly in excess of the coercive force E_c for the used material. In the case of the available equipment, and considering the material data which indicates that the coercive electric field is 45 $V/\mu m$, it is possible to process PVDF layers up to 4 μm.

After series of trials, it was discovered that the best way to perform the poling was at a very low frequency ($50 mHz$) and with a ramped sinusoidal waveform at a field slightly above the coercive force for films that were 1.9 μm thick. In the image 6.32 the behavior of the polarization current and the effect of the ferroelectric material is shown with the increase of the voltage of the applied varying field.

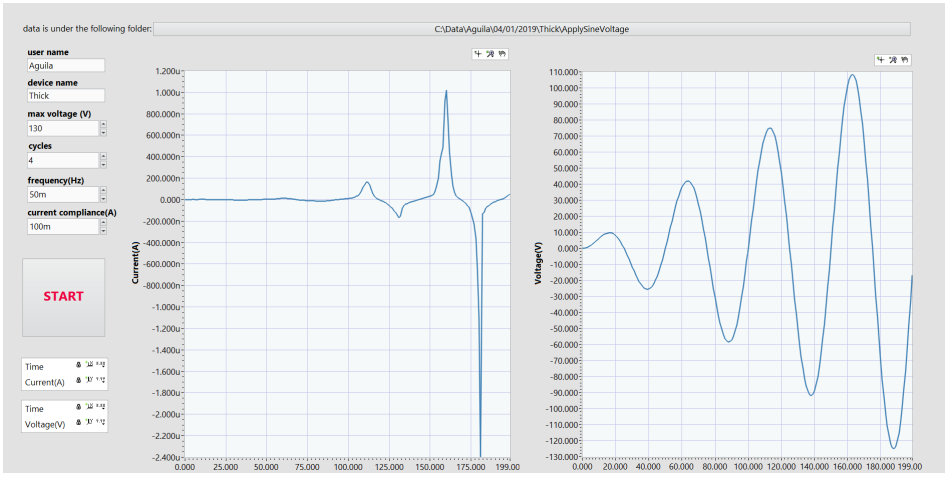

Figure 6.32: LabView application for poling

Chapter 7

Design of sensor

After processing PVDF, analyzing its properties and showing routes how to improve these, the final demonstration in this thesis is to build a functional sensor. For this purpose, a design is required based on the experiences accumulated during the performed experiments. At first glass substrates were used which were later exchanged for Kapton foil to apply greater stresses without damaging the device and to show its relevance for use in flexible sensor skins. Astoundingly, the latter approach was also preferable as it became much easier to fabricate the device due to the adhesion of epoxies and cyanoacrylates to the polymer substrate material. The use of Kapton film also matches with the newer applications, like the mentioned sensor skin, that demand high deformation, high forces and reliable long lasting material properties. Here, the sensor should be capable to withstand slight touching up to high impact forces.

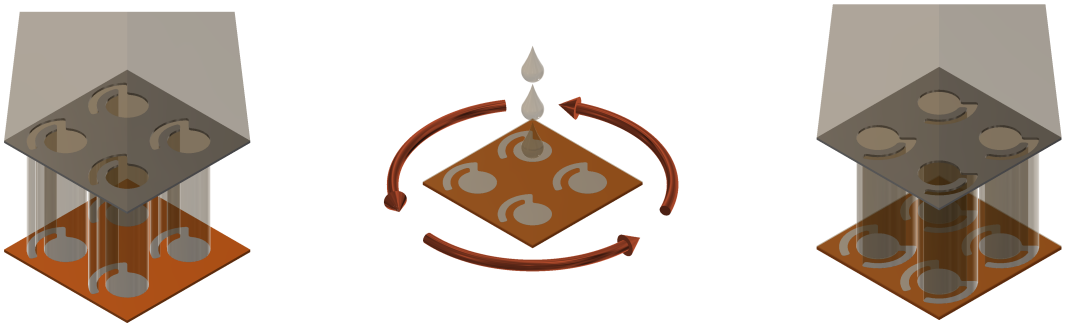

Figure 7.1: Fabrication process for sensor, the electrodes are fabricated through shadow masked sputtering, the PVDF-TrFE active layer is cast through spin-coating techniques and a last electrode is sputtered

The design of a simple device, based on the so far analyzed processes, was fabricated using Inventor. The bottom electrode was sputtered through a shadow mask onto the Kapton foil. Afterwards, the whole developed process run using PVDF-TrFE was performed. In detail, the material was spin coated at 3000RPM and baked at 135°C. Then the top electrode was again deposited using a shadow mask process. The resulting device had a PVDF layer of 1.9μm between 200nm thick electrodes on a Kapton foil.

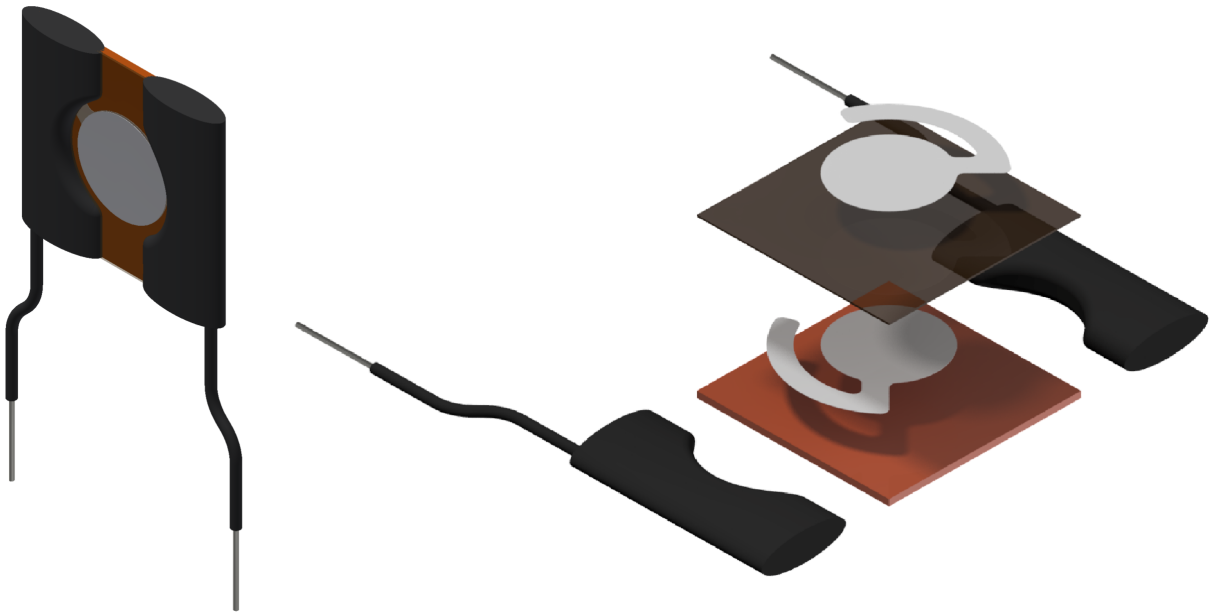

Figure 7.2: The final sensor has wires added with cyanoacrilate glue and conductive carbon paste, the exploded view (right) shows the layers in the following order: Kapton substrate, aluminum bottom electrode ($200nm$), PVDF film ($1.9\mu m$), aluminum upper electrode ($200nm$)

For electrical connection cables were fixed mechanically to the Kapton substrate with cyanoacrylate glue and then contacted electrically with carbon glue. The final device is shown in image 7.2. After fabrication the devices were poled with the help of a *Keithley 2400* sourcemeter with the process described above.

7.1. Electrical response

For this section, the electrical response of the transducer was tested. To test the device, the samples first were placed on a custom designed, sample holder connected to the MDO-2104EX, the signals achieved through tapping over the samples were registered to measure peak voltages of between 0.6 and 1.5 volts.

In the figures 7.3 in the upper position the reaction of the sensor when dropping object of 10 grams from a height of 5cm onto its active area (blue) and from 10cm height (red), it is possible to observe an oscillatory behavior which is characteristic for the electrical response of the material. The red curve features a higher signal amplitude of 0.6V, whereas the blue curve shows a smaller amplitude.

In the lower graph it is possible to observe a peak of 1.5 volts, the measured response using a perpendicular impact stimulus using a pen to deliver the force. The higher voltage arises from the qualitatively higher impact and shows a remarkable voltage that might be used without additional amplification circuits in a sensor array.

As a last test to demonstrate qualitatively the pyroelectric behavior a flow of warm air was applied over the surface of the sensor. The PVDF-TrFE device showed a response to the varying temperature of the flow which is shown in figure 7.5.

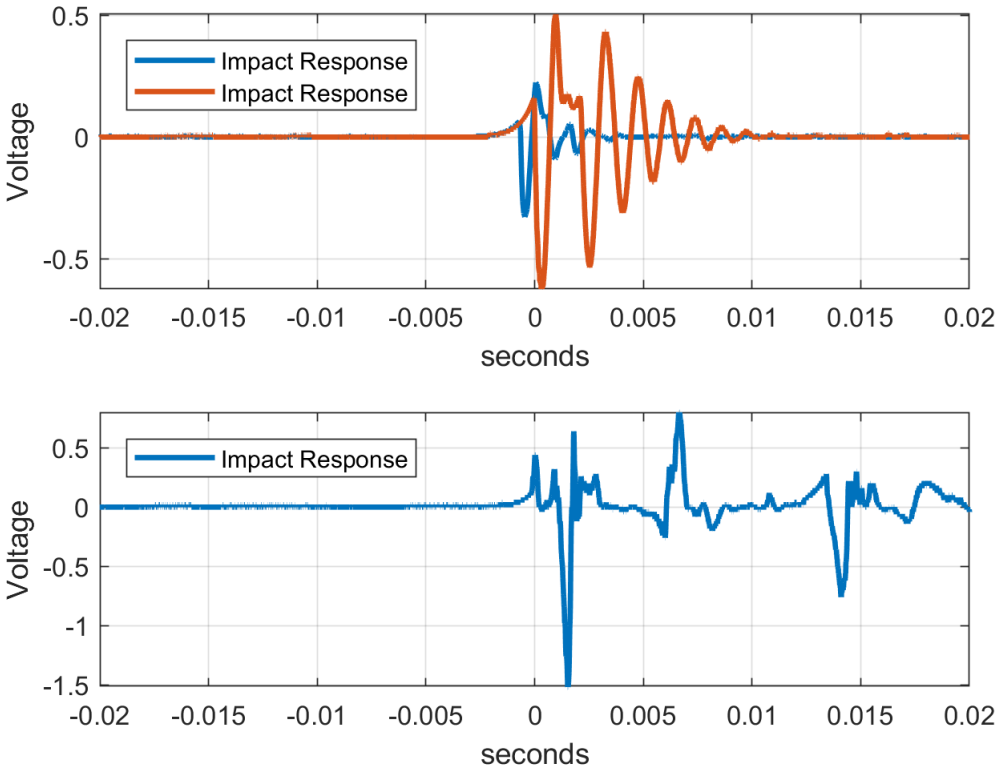

Figure 7.3: Electrical response, the sensor reacts delivering a voltage into its terminals after receiving an impact over the active area

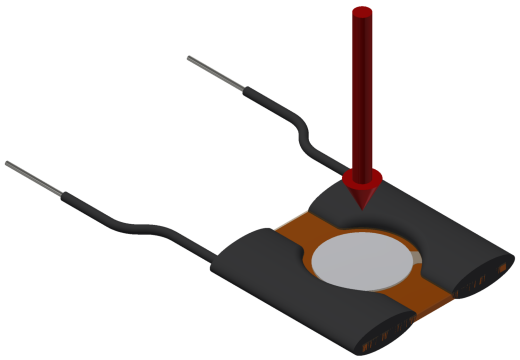

Figure 7.4: The sensing element receives a stimulus through the sudden application of force or pressure over the active area, piezo sensors don't have bias, then it is expected to only sense fast transitory changes

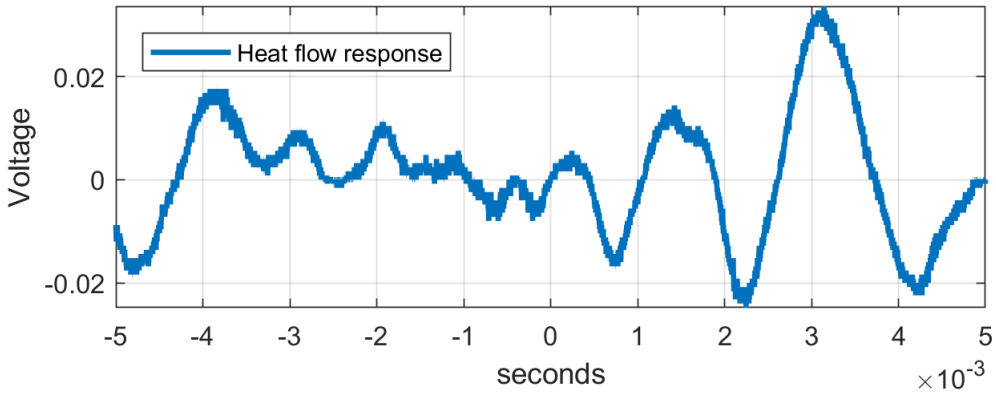

Figure 7.5: The sensor is also capable of detect changes in temperature, the graph shows the response of the sensor induced by a flow of warm air

7.2. Signal conditioning

Normal output voltages from piezoelectric sensors can vary from microvolts for single layer devices to hundreds of volts for multilayer or thick materials. For most applications and specific conditions, a signal conditioning is normally required. The main parameters to consider when designing an amplifier are:

- Frequency of operation
- Signal amplitude
- Input impedance
- Mode of operation

When a sensor has a high-output impedance it also requires an amplifier with high-input impedance. Here, JFET or CMOS input op amps are the preferred choices [33]. Two circuits can be used for signal conditioning for such sensors based on voltage mode and charge mode amplifiers. The voltage mode amplifier is commonly used when it in close proximity to the sensor. Charge mode amplification is used for amplifiers at a remote place.
In a voltage mode amplifier, the output depends on the amount of capacitance (seen) by the sensor. The capacitance associated with the interface cable will affect the output voltage, so consequently, if the cable is moved or replaced, variations in the interface cable capacitance can cause significant problems.

The charge mode amplifier will balance the charge injected into the negative input by charging the feedback capacitor. The resistor will bleed the charge of the feedback capacitor at a low rate to prevent the amplifier from drifting into saturation. The action of the amplifier maintains 0 V across its input terminals, so that the stray capacitance associated with interface cabling does not pose a problem [34].

According to the criteria mentioned before the selected amplifier to use in combination with the sensor should be the charge amplifier. Op amp selected was the TL082. This device has dual JFET input with an internally trimmed input offset voltage and has a high input impedance ($10^{12}\Omega$). The circuit was designed to be fed with $\pm$ 15 Volts, the design counts with a feedback capacitor of 1 $M\Omega$ and a capacitor of 33 pF. It can be seen in figure 7.7 that the signal shown in 7.3 has already been processed. It has been amplified and transformed into a smooth impulse response signal with a recovering time less than 0.2 milliseconds.

For the calculation of the amplifier gain the equation 7.1

$$Gain = \frac{1}{C_{FB}} = (mV/C) \tag{7.1}$$

For the calculation of the bandwidth it can be easily calculated as a high pass filter with the equation 7.2

$$f_{HPF} = \frac{1}{2\pi R_{FB} C_{FB}} \tag{7.2}$$

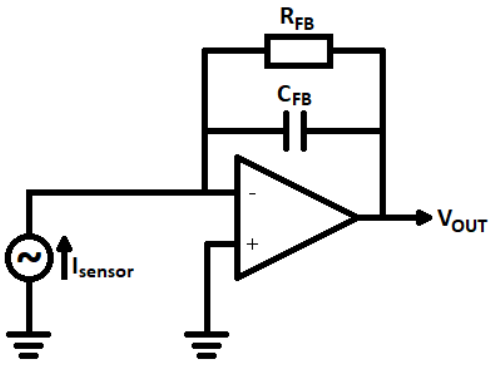

Figure 7.6: Amplifier schematic diagram

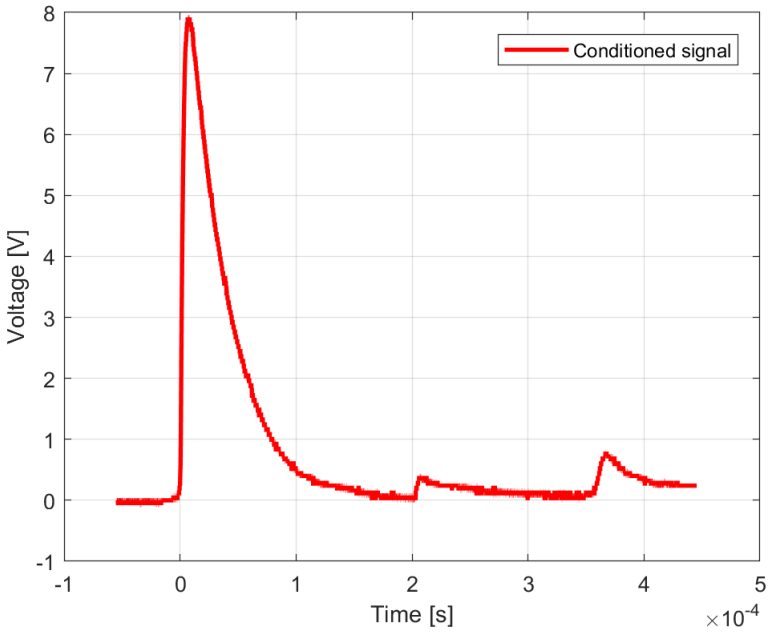

Figure 7.7: Signal conditioning: the signal is filtered and amplified by a charge amplifier

Chapter 8

Conclusions

PVDF is a versatile polymer that exhibits ferroelectric properties. As such, the material may be used as transducer to either detect changes of temperature or pressure or to function as actuator if a potential is applied. The core of this work was to find process routes to fabricate and test two PVDF materials on their functionality. Routes for processing the PVDF materials were developed, starting with basic test on solubility of the test materials followed by depositions tests. The materials were studied during the different procedures by microscope and Raman Spectroscopy, finding, that the used PVDF-TrFE was likely to have superior ferroelectric properties. The materials were integrated into the process flow of standard semiconductor fabrication methods and tested for their processability. Here, especially the formation of the PVDF-layer and the deposition of contacts was tested for different device sizes. The results of the emerging process routes were analyzed by SEM and then electrically characterized. Here, the measurements, using self-build circuits, showed, that the two PVDF materials demonstrated a completely different behavior, with the PVDF-TrFE showing a clear ferroelectric hysteresis while the standard PVDF showed only negligible functionalities; as was suspected from the performed spectroscopic Raman measurements. The superior PVDF-TrFE was then used in a modified poling procedure, set up on modified testing equipment at AMO, and integrated into a sensor concept. The resulting sensors were tested with self-build improvised circuits in combination with standard equipment. The device was successfully tested for the ferroelectric response and for an electrical response to stimulus by impact and temperature changes. The response of the sensor achieved a desired value, higher than the values found in the literature even without an amplification stage. The response of the sensor achieved desired values, higher than the values found in the literature even without an amplification stage. Last but not least, a simple circuit for the signal processing of the sensors was developed and used with the sensor device. From the performed analysis and accumulated experience, it can be concluded, that the PVDF-TrFE was the vastly superior material. It can be integrated into fabrication procedures that use standard semiconductor equipment, which is still dominant for the production of standard impact or pyro-sensors. Likewise, the exemplary fabrication on Kapton foil, shows significant potential for the formation of polymeric sensors and actuators for flexible sensor skins for fields ranging from straight forward automotive applications to relevant human-robotics security interfaces.

8.1. Further Work

- Improve on the fabrication of the device, better joining methods and materials should be taking into account to increase the resistance of the complete sensor while handling
- Perform encapsulation of the sensor in order to warrant better protection of the active area of the sensor without sacrificing the response of the device
- Development of integrated filters and amplification in a small package joining the active device all together
- Integration of the sensor films in ways they could be used for vibrational analysis and for acoustic or thermal measurements.
- Integration of micro-controllers in order to develop the PVDF-TrFE as an intelligent sensor

References

[1] Ravinder S. Dahiya. *Epidermal electronics: flexible electronics for biomedical applications*, pages 245–255. Cambridge University Press, 2015.

[2] Ravinder Dahiya. Electronic skin, March 2015.

[3] Ravinder Dahiya, Philipp Mittendorfer, Maurizio Valle, Gordon Cheng, and Vladimir J. Lumelsky. Directions toward effective utilization of tactile skin: A review. *Sensors Journal, IEEE*, 13:4121–4138, 11 2013.

[4] Chang Beom Eom and Susan Trolier McKinstry. Thin-film piezoelectric mems. *MRS Bulletin*, 37(11):1007–1017, 2012.

[5] Shoubhik Gupta, Flavio Giacomozzi, Hadi Heidari, Leandro Lorenzelli, and Ravinder Dahiya. Ultra-thin silicon based piezoelectric capacitive tactile sensor. *Procedia Engineering*, pages 662–665, 2016.

[6] Hari Singh Nalwa. *Ferroelectric Polymers: Chemistry, Physics, and Applications*. CRC Press, 1995.

[7] S. Gupta, H. Heidari, L. Lorenzelli, and R. Dahiya. Towards bendable piezoelectric oxide semiconductor field effect transistor based touch sensor. pages 345–348, May 2016.

[8] AMO GmbH. Sensor technology. Available: `https://www.amo.de/research/sensor-technology/` [Accessed: 28-Jan-2019].

[9] S. Kasap and Capper P. *Handbook of Electronic and Photonic Materials, vol. 53, no. 9*. 2013.

[10] C. R. Bowen, J. Taylor, E. LeBoulbar, D. Zabek, A. Chauhan, and R. Vaish. Pyroelectric materials and devices for energy harvesting applications. *Energy Environ. Sci*, pages 3836–3856, 2014.

[11] S. Choi and Y. Han. *Piezoelectric Actuators Control Applications of Smart Materials*. CRC Press, 2010.

[12] Encyclopaedia Britannica. Dielectric physics. Available: `https://www.britannica.com/science/dielectric` [Accessed: 11-Feb-2019].

[13] H. Kawai. Related content The Piezoelectricity of Poly (vinylidene Fluoride). *J. Appl. Phys.*, page 975, 1969.

[14] J. G. Bergman, J. H. McFee, and Crane G. R. Pyroelectricity and optical second harmonic generation in PVDF films. *Appl. Phys. Letts.*, 1971.

[15] A. Srinivasan and S. Bandyopadhyay. *Advances in polymer materials and technology.* CRC Press, 2016.

[16] H. Zhu, J. Matsui, S. Yamamoto, T. Miyashita, and M. Mitsuishi. Solvent-dependent properties of poly(vinylidene fluoride) monolayers at the air-water interface. *Soft Matter*, pages 1962–1972, 2015.

[17] Francois Bauer. Device for polarizing ferroelectric materials, August 4 1987. US Patent 4,684,337.

[18] T. R. Dargaville, M. C. Celina, J. M. Elliott, P. M. Chaplya, G. D. Jones, D. M. Mowery, R. A. Assink, R. L. Clough, and Martin J. W. Characterization, performance and optimization of PVDF as a piezoelectric film for advanced space mirror concepts. *Optimization*, 2005.

[19] M. Jones and S. A. Fleming. *Organic Chemistry.* Norton and Company, 2014.

[20] Louisiana State University. Polarity Index. Available: `http://macro.lsu.edu/howto/solvents/Polarityindex.htm`. [Accessed: 04-Jul-2018].

[21] S. Abbott. HSP for Beginners | Practical Solubility Science. Available: `https://www.stevenabbott.co.uk/practical-solubility/hsp-for-beginners.php`. [Accessed: 04-Jul-2018].

[22] S. Fakyrov. *Fundamentals of Polymer Science for Engineers.* Wiley, 2017.

[23] Fraunhofer Institute for Surface Engineering and Thin Films IST. Profilometry. Available: `https://www.ist.fraunhofer.de/en/our-services/film_surface_analysis/high_resolution_microscopy_surface_imaging/profilometry.html` [Accessed: 28-Jan-2019].

[24] Nanoscience Instruments. Nanoscience Instruments?:: How a Profilometer Works. Available: `https://www.nanoscience.com/technology/optical-profiler-technology/how-profilometer-works/`. [Accessed: 16-May-2018].

[25] R. Rijuta. Dektak 3ST Surface Profilometer. Available: `http://research.engineering.ucdavis.edu/cnm2/wp-content/uploads/sites/11/2016/02/CNM2_Dektak3ST-022016_final.pdf`. [Accessed: 18-May-2018].

[26] A. Busnaina. *Nanomanufacturing Handbook.* CRC Press, 2007.

[27] P. Larkin. *Çhapter 1 - Introduction: Infrared and Raman Spectroscopy,ïn Infrared and Raman Spectroscopy.* Elsevier, 2011.

[28] P. Larkin. *Çhapter 3: Instrumentation and Sampling Methods,ïn Infrared and Raman Spectroscopy.* Elsevier, 2011.

[29] R. Kumaran, M. Alagar, D. S. Kumar, V. Subramanian, and K. Dinakaran. Ag induced electromagnetic interference shielding of ag-graphite/pvdf flexible nanocomposites thin films. *Appl. Phys. Lett.*, 2015.

[30] R. Kumaran, M. Alagar, D. S. Kumar, V. Subramanian, and K. Dinakaran. The Investigation of Alpha to Beta Phase Transition in Poly(Vinylidene Fluoride) (PVDF). *12th International Symposium on Electrets*, pages 178–181, 2005.

[31] T. Boccaccio, A. Bottino, G. Capannelli, and P. Piaggio. Characterization of PVDF membranes by vibrational spectroscopy. *J. Memb. Sci.*, pages 315–329, 2005.

[32] I. S. Elashmawi and L. H. Gaabour. Raman, morphology and electrical behavior of nanocomposites based on peo/pvdf with multi-walled carbon nanotubes. *Results Phys.*, pages 105–110, 2015.

[33] James Karki. Signal conditioning piezoelectric sensors. Available: `https://www.ti.com/lit/an/sloa033a/sloa033a.pdf` [Accessed: 28-Jan-2019].

[34] Eduardo Bartolome. Signal conditioning for piezoelectric sensors. Available: `http://www.ti.com/lit/an/slyt369/slyt369.pdf` [Accessed: 28-Jan-2019].

Appendix A

Shadow mask designs

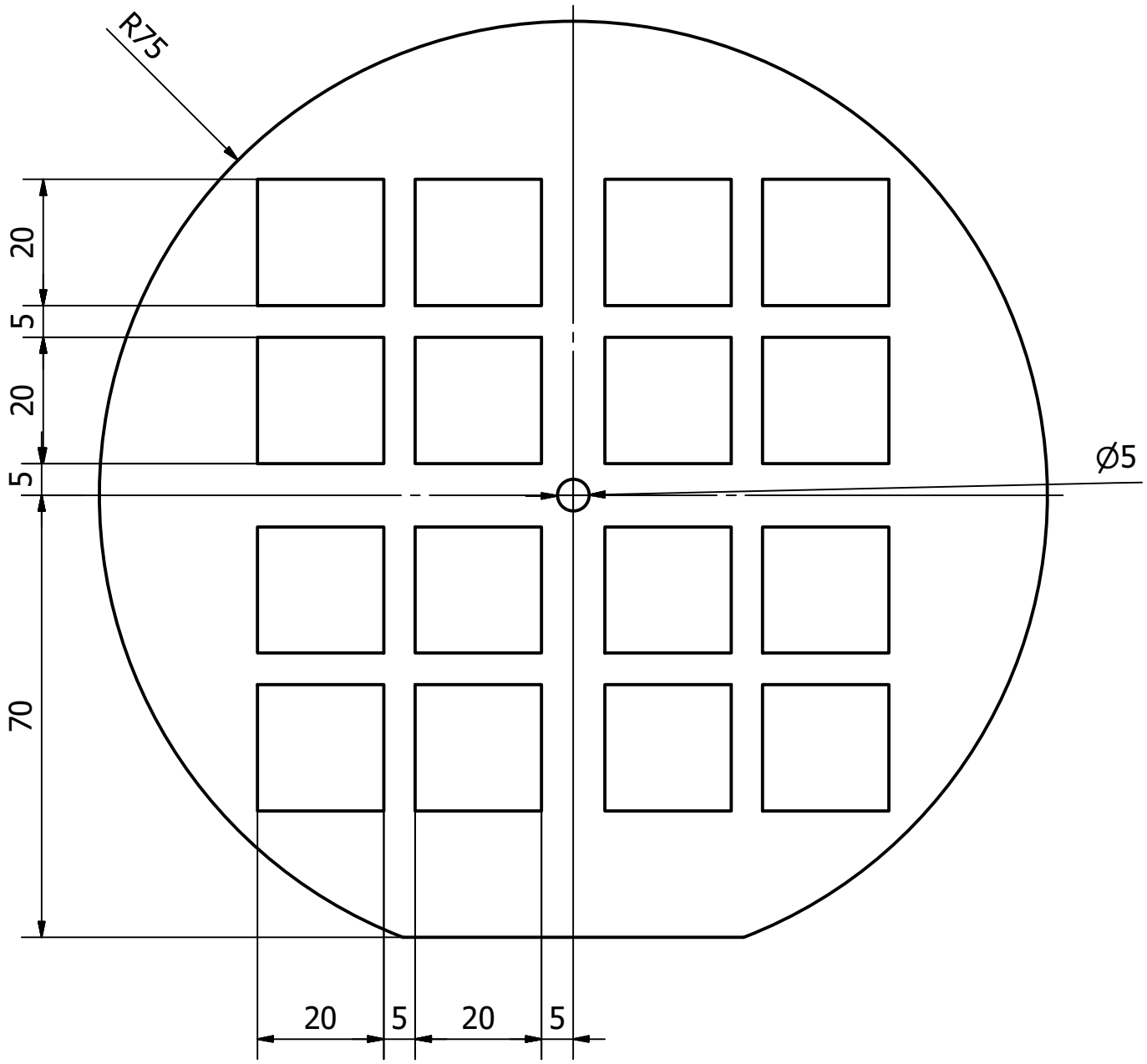

Diseño de	Revisado por	Aprobado por	Fecha		Fecha	
Gonzalo Aguila					12/09/2018	

samplepositioner		Edición	Hoja 1 / 1

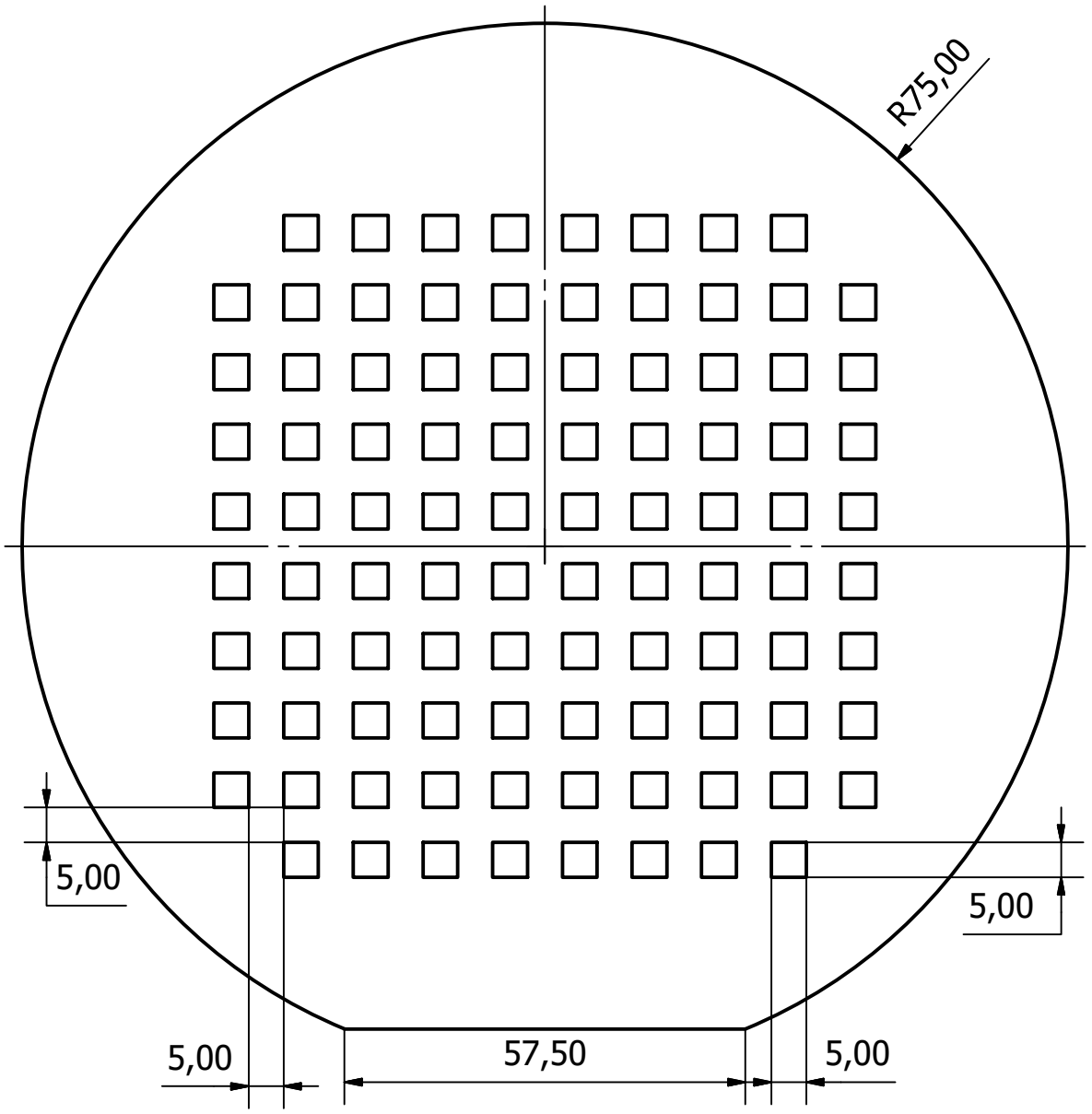

Diseño de	Revisado por	Aprobado por	Fecha		Fecha	
Gonzalo Aguila					07/08/2018	

SputteringMask5x5		Edición	Hoja 1 / 1

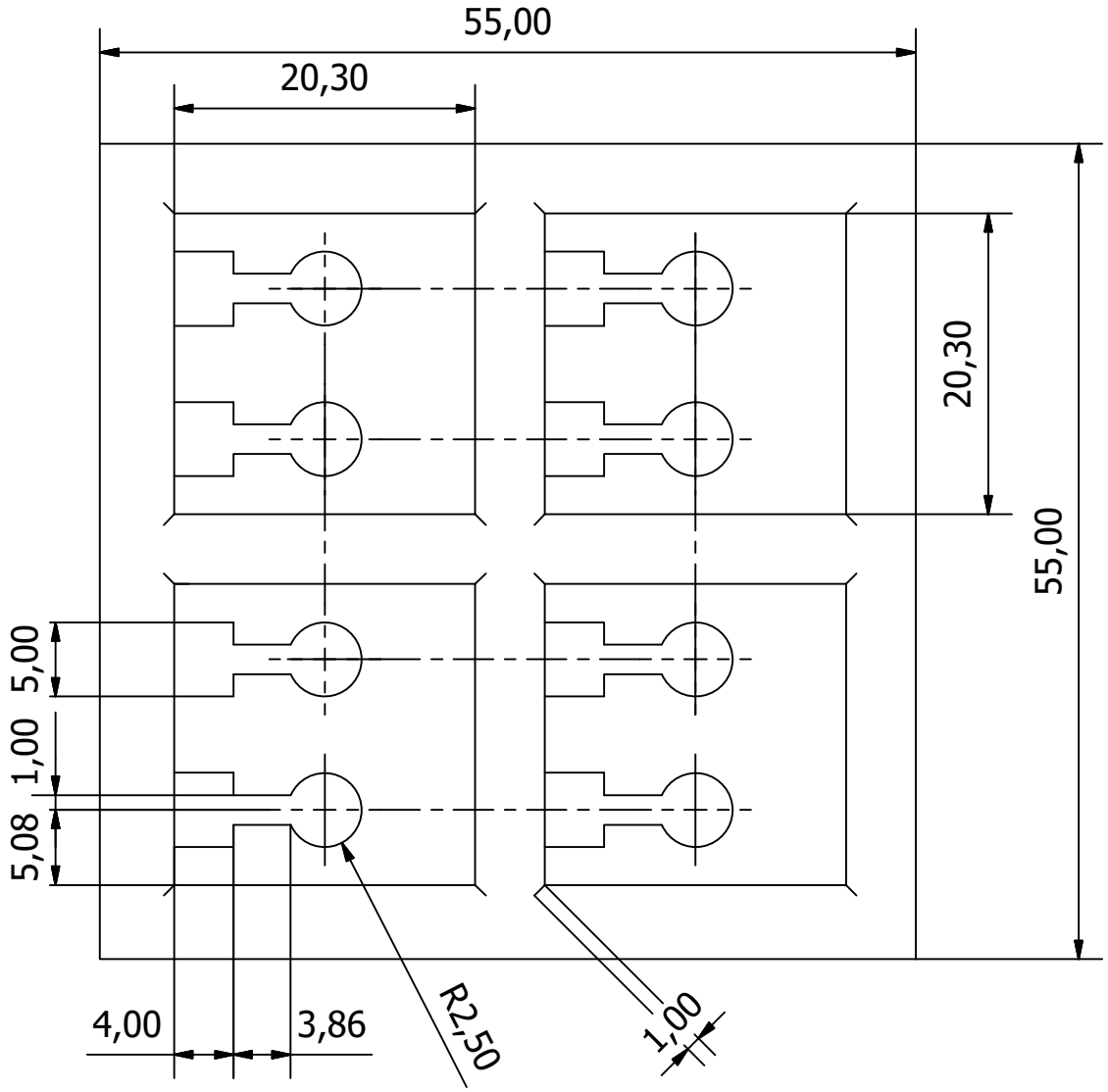

Diseño de	Revisado por	Aprobado por	Fecha		Fecha	
Gonzalo Aguila					17/12/2018	

circle5mm_matrix		Edición	Hoja 1 / 1

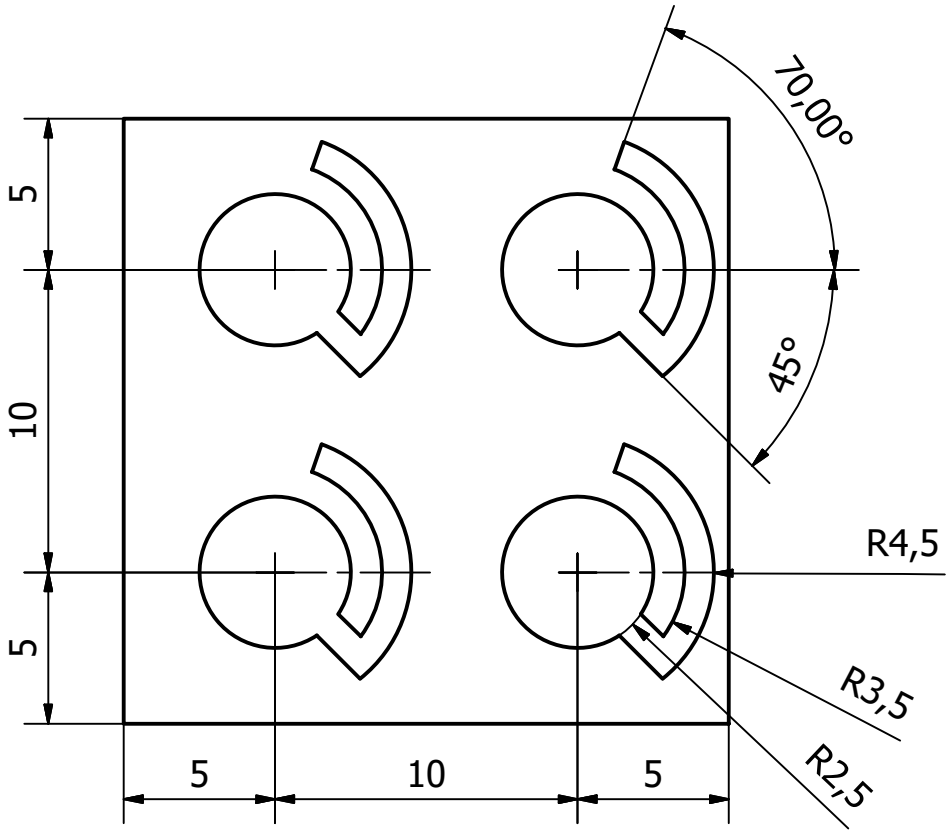

Diseño de	Revisado por	Aprobado por	Fecha		Fecha	
Gonzalo Aguila					11/09/2018	

electrode5d		Edición	Hoja 1 / 1